Constraints on the duration of the early Toarcian T-OAE and evidence for carbon-reservoir change from the High Atlas (Morocco)

Slah Boulila, Bruno Galbrun, Driss Sadki, Silvia Gardin, Annachiara Bartolini

BOULILA B., GALBRUN B., SADKI D., GARDIN S. & BARTOLINI A. (2019) - Constraints on the duration of the early Toarcian T-OAE and evidence for carbon-reservoir change from the High Atlas (Morocco). *Global Planetary Change*, 175, 113-128.

Constraints on the duration of the early Toarcian T-OAE and evidence for carbon-reservoir change from the High Atlas (Morocco)

Slah Boulila [1,2,*], Bruno Galbrun [1], Driss Sadki [3], Silvia Gardin [4], Annachiara Bartolini [4]

[1] Sorbonne Université, CNRS, Institut des Sciences de la Terre Paris, ISTeP, F-75005 Paris, France.
[2] ASD/IMCCE, CNRS-UMR8028, Observatoire de Paris, PSL University, Sorbonne Université, 77 Avenue Denfert-Rochereau, 75014 Paris, France.
[3] Moulay Ismaïl University, Faculty of Science, Department of Geology, BP. 11201 Zitoune, 50070 Meknes, Morocco.
[4] Sorbonne Université, MNHN, CNRS, Centre de Recherche sur la Paléobiodiversité et les Paléoenvironnements, CR2P, F-75005 Paris, France.

* Corresponding author. Tel.: +33 144274163; Fax: +33 144273831

Email addresses: slah.boulila@sorbonne-universite.fr (S. Boulila), bruno.galbrun@sorbonne-universite.fr (B. Galbrun), driss.sadki@gmail.com (D. Sadki), silvia.gardin@sorbonne-universite.fr (S. Gardin), bartolini@mnhn.fr (A. Bartolini)

Abstract

The Toarcian oceanic anoxic event (T-OAE, ~183 Ma) marks a geologically brief and severe global warming, associated with a profound perturbation in the global carbon cycle. The carbon cycle perturbation has been documented worldwide in marine and continental sedimentary records with a pronounced negative carbon isotope excursion (CIE) in the long-term $d^{13}C$ profile. However, the cyclostratigraphically inferred duration of the CIE, which was mainly derived from the Paris (France) and Lusitanian (Portugal) basins, remains controversial, resulting in two notably different estimates of 300-500 and 900 kyr.

Here, we present an early Toarcian cyclostratigraphic record from the High Atlas in Morocco (Talghemt section), based on high-resolution $d^{13}C$ and $\%CaCO_3$ data, which capture the Pliensbachian-Toarcian (Pl-To) transition event and the T-OAE, and strongly correlate to previous $d^{13}C$ key records. Orbital tuning based on the short and long, stable 405 kyr (g2-g5) eccentricity cycles, provides a duration of ~400 to ~500 kyr for the T-OAE. This duration is very close to that previously inferred from the Sancerre Core in the Paris Basin (300 to 500 kyr), and similar to that recently revised from the Peniche section (Lusitanian Basin, Portugal) (~472 kyr).

In addition, the 405 kyr $\%CaCO_3$ timescale at Talghemt calibrates high-frequency $d^{13}C$ variations at the Pl-To transition and the initiation part of the T-OAE to the obliquity cycle band, thus concuring with previous studies for obliquity forcing during these time intervals. The 405 kyr calibrated O1 obliquity period (~30 kyr) is shorter than the astronomically predicted one (~35 kyr), hence supporting the hypothesis of shortened obliquity periods during the Early Jurassic, and providing constraints on Earth's tidal dissipation factor during this geologic epoch.

Finally, a remarkable phase change between $\%CaCO_3$ and $d^{13}C$ orbitally paced cycles is observed for the first time at the T-OAE, suggesting a change in the carbon reservoir in relation with volcanically released greenhouse gases and major carbonate crisis. However, this phase shift is not observed at the Pl-To event implying different causal mechanisms on the carbon cycle perturbation between the Pl-To and T-OAE events.

Keywords: T-OAE, Pliensbachian-Toarcian transition, High Atlas, Morocco, astronomical timescale, obliquity, carbon cycle, volcanic greenhouse gases.

Introduction

The early Toarcian oceanic anoxic event (T-OAE, Jenkyns, 1988) documents one of the most important perturbations in the global carbon cycle during the Phanerozoic eon, expressed in marine and continental carbon isotopic data ($d^{13}C$) as a negative carbon isotope excursion (CIE) (e.g., Duarte, 1998; Hesselbo et al., 2000). Accompanying the carbon cycle perturbation are profound modifications in other geochemical cycles (Gill et al., 2011; Montero-Serrano et al., 2015), in the hydrological cycle (Cohen et al., 2004; Cohen and Coe, 2007; Bodin et al. 2011; Brazier et al. 2015; Krencker et al., 2015; Montero-Serrano et al., 2015; Them et al., 2017a; Izumi et al., 2018), and in biotic cycling marked by a biomass crisis affecting marine invertebrate macrospecies and biocalcifying organisms (Harries and Little , 1999; Macchioni and Cecca, 2002; Wignall et al. 2005; Gomez et al. 2008; Mattioli et al. 2008; Suan et al. 2008a; Dera et al., 2010; Caruthers et al., 2013, 2014; Clémence et al., 2015, and others).

Timing and duration of the T-OAE is crucial for the determination of magnitudes and rates of the associated geological processes. Astrochronology is today an emerging approach to measure geologic times with a good precision (e.g., Hinnov, 2013) in successions devoid of volcanic ash beds, in conjunction with other classical dating methods (e.g., McArthur et al., 2000; Sell et al., 2014; Burgess et al., 2015). However, current cyclostratigraphic studies show considerable differences in cycle interpretation, and thus in the duration of CIE associated to the T-OAE. The cyclostratigraphically inferred duration of CIE ranges from 300 to 900 kyr (Suan et al., 2008b; Boulila et al., 2014; Huang and Hesselbo, 2014; Boulila and Hinnov, 2017).

The establishment of a precise astronomical timescale for the T-OAE also allows quantification of the pronounced short-term $d^{13}C$ oscillations within the decreasing part of CIE, the origin of which has still been controversial (see Boulila and Hinnov, 2017, and references therein). These short-term $d^{13}C$ oscillations are of particular interest because they may reflect phases of massive dissociation of gas hydrate and/or of enhanced terrestrial methanogenesis (Hesselbo et al., 2000; Kemp et al., 2005 ; Hesselbo and Pienkowski, 2011 ; Them et al., 2017b, Ikeda et al., 2018), or amplified astronomical cycles mediated by volcanically released greenhouse gases (Boulila and Hinnov, 2017). Significant biomass decline events were also recognized at these short-term $d^{13}C$ oscillations (e.g., Harries and Little, 1999). In addition, the Pliensbachian-Toarcian (Pl-To) transition records a negative CIE, associated with a significant biodiversity drop (disappearance of upwards 90% of the global ammonite taxa, Dera et al., 2010) and a conspicuous nannofossil turnover (Erba, 2006). It is also marked by a widespread sedimentary gap caused by a severe regression and cooling event (Guex et al., 2001, 2016; Dera et al., 2009, 2011; Caruthers et al., 2013, 2014; Suan et al., 2011). The T-OAE is coeval to a second extinction event affecting mainly benthic fauna (foraminifera, bachiopods, etc) (Bartolini et al., 1992; Joral et al., 2011; Danise et al., 2015), during quite different paleoenvironmental conditions of super-greenhouse, transgression and anoxia (e.g., Suan et al., 2011).

Here, we present high-resolution bulk carbonate $d^{13}C$ and carbonate content data from an early Toarcian sedimentary (Talghemt) section situated in the High Atlas of Morocco, which covers the Pliensbachian-Toarcian transition and the totality of T-OAE. The main objectives of the present study are (i) to resolve the controversies on the duration of T-OAE, (ii) to assess the periodicity of the prominent short-term $d^{13}C$ oscillations focused on the decreasing part of CIE, and (iii) to discuss their potential paleoenvironmental implications.

1. Material and methods

1.1. Geological setting and biostratigraphic framework of the Talghemt section

The Talghemt section is situated in the northeastern part of the central High Atlas of Morocco (N32°35'34"-W04°31'03"), 25 km from Midelt town (Fig. 1), and crops out along the main road '*Route Nationale RN13*' joining Midelt to Rich (Dubar, 1932; El Hariri, 1990; Sadki, 1996). It was located on a paleo-high in the basinal High Atlas realm, called the "*Ride*" of Talghemt (e.g., Sadki, 1996; El Kamar et al., 1997).

The Talghemt outcrops offer one of the best sedimentary records of the Pliensbachian-Toarcian transition in the Tethyan realm. The Talghemt sedimentary successsion was previously proposed as a candidate section for the Toarcian GSSP (Global Boundary Stratotype Section and Point) (Elmi, 2006) given its richness in ammonite fauna and also because of the excellent quality of outcrops and the easy access to the strata.

A detailed stratigraphic description of the Talghemt section is provided in Figure 2 and Section 1.2. The Pliensbachian-Toarcian transition is composed of marl-limestone alternations of the Ouchbis Formation (Studer, 1980) (Fig. 2A,C). The limestone beds and marly levels are numbered as in Sadki

(1996), with even numbers for limestones and odd numbers for marls. Beds numbered TdB8 through TdB28 exhibit large-sized ammonites of the Pliensbachian Emaciatum Zone (Fig. 2C and Plate 1). We can distinguish the two following parts (Sadki, 1996): (i) the lower part with *Emaciaticeras* (TdB8 through TdB14), which contains *Emaciaticeras emaciatum* (Catullo), *E. imitator* (Fucini), *E. lottii* (Gemmellaro), *Emaciaticeras* sp., *Canavaria zancleana* (Fucini), *C.* (*Naxensiceras*) *depravata* (Fucini), *Canavaria* sp., *Lioceratoides lorioli* (Bettoni), *Lioceratoides* sp., *Phylloceras* sp., and (ii) the upper part with *Tauromeniceras* (TdB15 through TdB28), which contains *Taurominеceras nerinum* (Fucini), *Taurominеceras* cf. *nerinum* (Fucini), *T. mazetieri* (Dubar), *Tauromeniceras* sp., *Emaciaticeras gracile* (Fucini), *Neolioceratoides* gr. *Hoffmanni* (Gemmellaro), *Paltarpites* sp., *Lytoceras* sp., and *Phylloceras* sp.

The uppermost marly level TdB29 and limestone bed TdB30 contain ammonite fauna of the Toarcian Polymorphum Zone (Fig. 2C and Plate 2): *Eodactylites simplex* (Fucini), *E. mirabilis* (Fucini), *E. pseudocommunis* (Fucini), *Eodactylites* sp cf. *E. polymorphum* (Fucini), *Eodactylites* sp., and some forms already known since the Upper Pliensbachian [*Paltarpites paltum* (Buckman)], *Paltarpites* sp., *Neolioceratoides* gr. *Hoffmanni* (Gemmellaro).

The marl-limestone alternations are overlain by thick silty marls of the Tagoutite Formation (Studer, 1980) (Fig. 2A,B), and ~~but~~ characterized by an ammonite fauna comprising some *Eodactylites simplex* (Fucini) and *Eodactylites* sp. (Plate 2)

A first micropaleontological study based on foraminifera and ostracod analyses was provided by El Kamar et al. (1998). In this study, we investigate calcareous nannofossil analyses as follows. Ten samples from the upper Pliensbachian, and 68 samples from the lower Toarcian were processed as simple smear slides according to the standard procedure and analyzed by a Zeiss imaging II polarising microscope at 1500X. No less than three traverses of the slide (more than 300 fields of view) were thoroughly analysed and key taxa were quantified (Plate 3 and Fig. 3). Calcareous nannofossils are present along the studied section although in low abundance and their preservation is always poor. Assemblages are characterized by common *Calcivascularis jansae*, *Schizosphaerella* spp., *Lotharingius*, *Biscutum* and *Calyculus* (Plate 3).

Despite the low abundance and poor preservation, some important bio-horizons could be highlighted (Fig. 3). *Lotharingius sigillatus* is present from the base of the section but specimens exceeding 5 µm are observed at 5.80 m. *Carinolithus poulnabronei* were first observed at 8.1 m, at the base of Polymorphum Zone. *Crucirhabdus primulus* last occurs around 21 m within the Polymorphum Zone. The first reliable specimens of *Carinolithus superbus* were recorded around 29 m in the upper part of the Polymorphum Zone. The last *Parhabdolithus liasicus* was recorded around 37 m in the Levisoni Zone. One specimen of *Discorhabdus striatus* at 33.9 m, and three specimens of *Discorhabdus ignotus* at 20, 21.70 and 33.9 m were also encountered, but their lowest abundance and very scattered occurrence prevented confident definition of a bio-horizon.

Despite the low abundance, the non continuous occurrence and the poor preservation of calcareous nannofossils, the succession of bio-horizons recorded at Talghemt is consistent with those found in other Tethyan and Boreal basins as reported by Kaenel et al (1996), and Mattioli and Erba (1999) and helps to strengthen the biostratigraphic framework provided by ammonites.

1.2. Lithological and sedimentological data

The studied stratigraphic interval of the Talghemt section is ~69 m thick, and encompasses the Pliensbachian-Toarcian transition and early Toarcian pelagic sediments (Fig. 2B).

The lowermost part (0-8 m) of the section (Fig. 2B,C), at the Pliensbachian-Toarcian transition, is composed of marl-limestone alternations. The rest of the section, within the Polymorphum and Levisoni ammonite zones, consists of carbonate-rich clays. In detail, the interval from 8 to 29.1 m consists of homogeneous carbonate-rich clays. Then, the interval from 29.1 to 48.3 m presents carbonate-rich clays with frequent intercalations of mm- to cm-scale turbidite levels, and with three dm-scale turbidite levels at around 30.8, 38.2 and 38.7 m, and another thickest (25 cm) turbidite level, situated at around 42.8 m. The section crops out into two close parts, bounded at 48.5 m by a ~5 cm thick turbidite level, which was suspected to be a fault surface (e.g., Sadki, 1996, indicated by an arrow in Figs. 2 and 3). However, there is not any feature of a fault in the outcrops, and in addition geochemical data do not indicate any abrupt change at the suspected fault (Figs. 3 ad S1). Thus, we discard the hypothesis of a fault or at least the effects of a possible fault on the stratigraphic continuity at this level. The overlying interval (48.5 to 69 m) consists of homogeneous carbonate-rich clays with only two levels of turbidite intercalations at 61 and 68 m.

1.3. Sampling and geochemical data for cyclostratigraphy

The Talghemt section was sampled with an average space of 6 cm for the interval from 0 to

48.35 m, and an average space of 15 cm for the interval from 48.35 to 69 m (turbidite levels were not sampled). Such high-resolution sampling resulted in 930 samples. The whole samples were measured for carbonate content (%$CaCO_3$) following the volumetric method employing a Bernard calcimeter (uncertainties lower than 0.5%). The half of the collected samples (i.e., 465 samples, one every two samples) were measured for bulk stable carbon isotopes ($d^{13}C$). The analyses were performed at the SSMIM (Service de Spectrométrie de Masse Isotopique du Muséum National d'Histoire Naturelle de Paris, France) using a Delta V Advantage isotope ratio gas mass spectrometer (Thermofischer Scientific) which was directly coupled to a Kiel IV automatic carbonate preparation device (reaction at 70 °C under vacuum) and calibrated via NIST 19 to the VPDB (Vienna Pee Dee Belemnite) scale. The overall precision of the measurements was better than 0.03 and 0.04% for carbon and oxygen, respectively. The precision of $d^{13}C$ measurements, estimated as the standard deviation of the mean calculated for replicate analyses, is ±0.03‰.

High-resolution %$CaCO_3$ and $d^{13}C$ data are described below (Section 2.1), then treated to seek for cyclicities via the multitaper method (MTM) spectral analysis (Thomson, 1982) (Section 2.1). Prior to spectral analysis, data were detrended using the weighted-average lowess method (Cleveland, 1979) (30% for $d^{13}C$ and 15% for %$CaCO_3$). The MTM spectra were conducted using three 2p tapers, together with the robust red noise test (Mann and Lees, 1996). We used the gaussian filter (Paillard et al., 1996) to extract the dominant sedimentary cycles. Finally, we tuned the data using the stable 405 kyr eccentricity orbital parameter (Laskar et al., 2004), conjointly with the short eccentricity (mean 110 kyr) in order to assess the duration of the T-OAE.

2. Results

2.1. $CaCO_3$ and $d^{13}C$ data

High-resolution $d^{13}C$ data capture the two negative excursions of the Pliensbachian-Toarcian (Pl-To) and T-OAE events with amplitudes of 2.3% and 2.7% respectively (Figs. 3 and S1). A diagenetic imprint on $d^{13}C$ could not be excluded given the lighter $d^{13}C$ values along the Talghemt section, compared to other key records (e.g., Peniche, Hesselbo et al., 2007; Sancerre, Hermoso et al., 2009). However, the good correlation with other $d^{13}C$ key records suggest that the curve pattern at Pl-To and T-OAE events are not diagenetically obliterated (Section 3.1).

A possible interpretation of the extent of CIE of the T-OAE at Talghemt is thus proposed as minimum and maximum, depending especially on the end of CIE (Fig. 3). In addition to the detection of Pl-To and T-OAE events, $d^{13}C$ data show high-frequency cyclicities, which are explored in Section 2.2.

High-resolution $CaCO_3$ data show strongly cyclic variations at different wavelengths (Figs. 3 and 4). The Pliensbachian-Toarcian transition interval exhibits high-amplitude (~20 to ~70%) $CaCO_3$ cycles associated with the marl-limestone alternations. The marly interval of Polymorphum Zone shows cycles with weaker amplitudes, ranging from ~15 to ~40%. Interestingly, the lower part of the Levisoni Zone exhibits strong $CaCO_3$ fluctuations (~5 to ~60%), related to the T-OAE. Finally, the upper part of the Levisoni Zone, overlying the T-OAE interval, shows weaker cyclic variations (~15 to ~35%). All these $CaCO_3$ cyclicities are treated below via spectral analysis.

2.2. Time-series analysis

Spectral analysis of $CaCO_3$ and $d^{13}C$ data in the stratigraphic (m) domain shows multiple significant peaks (Fig. 4). The strongest, low-frequency peak is centred on 13 m in $CaCO_3$ and on 12.4 m in $d^{13}C$. Another possible common, dominant low-frequency peak is centred on 3.5 m in $CaCO_3$ and on 3.2 m in $d^{13}C$. High-frequency peaks are with weak powers, and range from ~0.3 to 1.8 m in $CaCO_3$ and from ~0.5 to 3.2 m in $d^{13}C$.

The above two low-frequency peaks have a wavelegth ratio of about ¼ implying a frequency ratio of short (110 kyr, mean of 95 and 125 kyr) and 405 kyr eccentricity. Accordingly, we interpreted the 12.4 and 13 m as reflecting the 405 kyr eccentricity cycle and the 3.2 and 3.5 m as the short eccentricity (110 kyr) cycle. Then, we tuned the $CaCO_3$ and $d^{13}C$ data to 405 and 110 kyr periods (Fig. 5). Spectral analysis of $CaCO_3$ and $d^{13}C$ data in the 405 kyr time domain (Fig. 5) calibrates the wavelegths of 3.2 and 3.5 m to periods of 106 and 118 kyr in $d^{13}C$ and $CaCO_3$, matching the short eccentricity cycle band.

Wavelengths of 0.3 to 1.8 m are tuned in part to precession and obliquity cycle bands. At these high frequencies, we can first note that the common peak at 1.8 m in $CaCO_3$ and $d^{13}C$ is tuned to 61 kyr, which persists strong in the tuned $CaCO_3$ but becomes very weak in the tuned $d^{13}C$. Such 61 kyr period does not match Milankovitch cycle band. The strong peaks at around 1 m are calibrated to periods of 30-33 kyr in the 405 kyr tuned $CaCO_3$ data (Fig. 5), which are shorter than the

astronomically (early Jurassic) predicted 35 kyr period (Laskar et al., 2004). In order to check this mismatch, we applied successive tunings at the obliquity band by changing its (target) period with a 1-kyr increment, and looking in parallel at the calibrated g2-g5 eccentricity term. The optimal obliquity target period that provides a 405 kyr period for g2-g5 orbital term (Laskar et al., 2004) is about 30 kyr, thus supporting a shorter obliquity period than that astronomically predicted, i.e. 35 kyr, for the Toarcian (Fig. 6).

Although the 405 kyr $d^{13}C$ tuning provides calibrated precession, obliquity and short eccentricity periods that are close to those in the 405 kyr $CaCO_3$, $d^{13}C$ filtering at the 405 kyr band does not show coherent cycle phase compared to 405 kyr $CaCO_3$ filtering (Fig. 7). We suspect that $d^{13}C$ trends from T-OAE and Pl-To events may have affected cyclic oscillations related to the 405 kyr cycles. Therefore, we retained only the 405 kyr tuning from $CaCO_3$ data.

Spectral analysis of the 110 kyr tuned $CaCO_3$ and $d^{13}C$ data provides consistent results with respect to the 405 kyr tuning. The long eccentricity is calibrated to 402 and 415 kyr in $CaCO_3$ and $d^{13}C$ respectively. The strongest obliquity related peaks are calibrated to 30-34 kyr and 29-31 kyr in $CaCO_3$ and $d^{13}C$ respectively, which are again shorter than the astronomically predicted 35 kyr period.

The 405 kyr tuning permits calibration of the duration of the T-OAE as ~400 kyr (minimum) and ~500 kyr (maximum) (Fig. 7). The pronounced high-frequency cycles expressed as marl-limestone alternations at the Pliensbachian-Toarcian transition are tuned to the obliquity cycle band (Figs. 4 and 5). The high-frequency cycles at the decreasing part of CIE are also calibrated to the obliquity band (Figs. 7 to 9). Finally, a striking change in the phase of cyclicities in $CaCO_3$ and $d^{13}C$ data has been noticed (Fig. 7), which may have potential implications for the carbon cycle during the T-OAE (discussed in Section 3.2).

3. Discussion

3.1. Correlation with previous T-OAE key records

A number of studies of the late Pliensbachian through the Toarcian have been conducted in the High Atlas of Morocco, and highlighted the Pliensbachian-Toarcian (Pl-To) and T-OAE events (Bodin et al., 2010, 2011, 2016; Krencker et al., 2014). A detailed $d^{13}C$ correlation between sections from the High Atlas Basin along with key records from other sites was provided by Bodin et al. (2016) (their Figure 8). In figure S2, we present a $d^{13}C$ correlation between Talghemt (the present study), and Boumardoul n'Imazighn and Amellago sections (Bodin et al., 2010, 2011, 2016) of the High Atlas in Morocco. Although there is a very likely diagenetic imprint in $d^{13}C$ data at Talghemt, correlation with Amellago indicates similar amplitudes within the T-OAE, ~2.7‰ at Talghemt (Section 2.1) and ~3‰ at Amellago (Bodin et al., 2010, 2016).

In addition, the amplitude of the $d^{13}C$ within the T-OAE between Talghemt and the Peniche reference section suggests similar trends, except at the '*Plateau*' interval. There could be a reduced '*Plateau*' or likely no '*Plateau*' at Talghemt (Fig. 8A). At Peniche, there are almost 2.5‰ $d^{13}C$ from the onset of T-OAE to the '*Plateau*', and almost 3‰ up to the first most significant shift. At Talghemt, we note 2.7‰ from the onset of T-OAE to the most significant shift. Thus, the 2.7‰ $d^{13}C$ amplitude at Talghemt is comparable to the 3‰ at Peniche.

Therefore, we suggest that the diagenetic imprint may affect the entire $d^{13}C$ signal at Talghemt towards lighter values, but does not alter the shape of CIEs of Pl-To and T-OAE events. A detailed $d^{13}C$ correlation between Talghemt and Peniche corroborates this hypothesis (Fig. 8A). Although we point out the preservation of the shape of CIEs at Talghemt, diagenetic processes could also alter the amplitude of CIEs. For instance, CIE associated with the T-OAE from other sections in NW Europe possesses an amplitude of more than 6‰ (e.g., Kemp et al., 2005, 2011; Hermoso et al., 2009).

The sedimentological and $d^{13}C$ data of the Talghemt and Peniche sections show several surprising similarities. The latest Pliensbachian and the Pliensbachian-Toarcian (Pl-To) transition are characterized by marl-limestone alternations in both sections, along with a remarkably negative $d^{13}C$ shift marking the Pl-To transition event.

Three main (thicker) turbidite levels are readily correlative. The two lower ones are situated within the T-OAE and the upper one is immediately above the T-OAE. Although Talghemt and Peniche sections show some common, main sedimentological and $d^{13}C$ features, implying similar depositional environments, we have to note that other previously studied basinal sections in the High Atlas do not show similar sedimentological and $d^{13}C$ features than Talghemt (Bodin et al., 2016, Fig. S2). It is very likely that the specific paleogeographic position of Talghemt at a paleo-high in the basin (e.g., Sadki, 1996; El Kamar et al., 1997) gives some different characteristics to this section, but the question remains open on the potential correlative turbidite levels with Peniche (Lusitanian basin).

We also propose a correlation with two other key $d^{13}C$ records at Sancerre (Paris Basin) and Yorkshire (UK) (Fig. 8B). The negative CIE associated with the PI-To transition event is recorded at Talghemt, Peniche and Yorkshire, but not at Sancerre. The CIE associated with the T-OAE share some features between the four sections. A detailed correlation of the decreasing part of CIE is provided in Section 3.3. Nevertheless, the remarkable difference in T-OAE CIE between the four records is the presence of a significant 'Plateau' at Peniche, which is not recorded at Sancerre, Yorkshire, and likely at Talghemt.

3.2. On the duration of T-OAE

The duration of the negative carbon isotope excursion (CIE) of the T-OAE (hereafter "the duration of the T-OAE") has been controversial during the last decade (Suan et al., 2008b; Kemp et al., 2011; Boulila et al., 2014; Huang and Hesselbo, 2014; Ruebsam et al., 2014; Boulila and Hinnov, 2015; Burgess et al., 2015; Boulila and Hinnov, 2017). Previous cyclostratigraphic estimates come mainly from NW European basins, and the Lusitanian Basin (Portugal) at Peniche. Two main cyclostratigraphically estimated durations of the T-OAE have been proposed. A first duration of 900 kyr was suggested by Suan et al. (2008b) on the basis of Peniche and Dotternhausen (SW Germany) sections, then supported later by Huang and Hesselbo (2014) using the same sections. A shorter duration of 300 to 500 kyr was suggested by Boulila et al. (2014) on the basis of Sancerre Core (Paris Basin), supporting the more likely option among the two cyclostratigraphic interpretations proposed by Kemp et al. (2011) on Yorkshire (England) and Peniche sections. Independent radioisotope geochronology (Sell et al., 2014; Burgess et al., 2015) favors a shorter duration, hence corroborating with cyclostratigraphic results of Kemp et al. (2011) and Boulila et al. (2014). A recent cyclostratigraphic review of the duration of T-OAE (Boulila and Hinnov, 2017) yields the shorter 300-500 kyr duration estimate, but still using the same sections, Sancerre and Peniche.

Cyclostratigraphically inferred duration estimates from Dotternhausen, Peniche and Yorkshire sections were based on high-frequency astronomical cycles (precession, obliquity and/or short eccentricity), likely because the studied intervals in these sections are not enough long to cover a sufficient number of low-frequency (405 kyr eccentricity) orbital cycles (e.g., Suan et al., 2008b; Kemp et al., 2005). The precession and obliquity periods are, however, very poorly constrained in the Mesozoic because of our limited knowledge on the tidal dissipation factor (see Section 2.2). The short eccentricity periods, resulting mostly from the orbital motion of the inner planets, are also subject to instabilities from the chaotic diffusion in the Solar System, and cannot be confidently used alone to tune the Mesozoic timescale (Laskar et al., 2004). The only reliable orbital eccentricity period that could be used to tune the Mesozoic timescale is the 405 kyr eccentricity (i.e., g2–g5) because it results from the gravitational interaction of Venus (g2) and Jupiter (g5), which have relatively stable orbits (Laskar et al., 2004).

Duration of the T-OAE at Sancerre was based on this 405 kyr stable eccentricity period, which is continuously recorded throughout 150 m thick succession encompassing the entire Toarcian stage (~8.3 Myr long) (Boulila et al., 2014). The Talghemt section presented here is an additional T-OAE record from another realm, and the first cyclostratigraphic T-OAE signal in the High Atlas domain, which documents the 405 kyr eccentricity. In particular, the $\%CaCO_3$ cyclostratigraphic signal documents with high fidelity both high- and low-frequency astronomical cycles. It is likely that diagenesis and turbidites may have some influence on high-frequency cycles, but less on the low-frequency ones, such as the 405 kyr eccentricity component, used here to tune the Talghemt record. The 405 kyr stable eccentricity conjointly with the short eccentricity tunings provide a duration of ~400 to ~500 kyr for the T-OAE, which is in excellent agreement with previous estimates from NW European basins (e.g., Boulila et al., 2014).

We should note that Huang and Hesselbo's (2014) T-OAE timescale is also based on the 405 kyr eccentricity cycle, retrieved from Peniche $d^{13}C$ data (their figure 3). In the present study, we point to the difficulty in extracting the 405 kyr eccentricity cycle from $d^{13}C$ record (Fig. 7). We suggest that the abrupt, severe $d^{13}C$ changes related to the PI-To and T-OAE events, in addition to the presence of the 'Plateau' within the T-OAE (and hiatuses at Peniche, e.g., Pittet et al., 2014), make the extraction of low-frequency (405 kyr) cycles unreliable. Unlike $d^{13}C$ data, the $\%CaCO_3$ profile is less sensitive to PI-To and T-OAE events, which was potentially used to calibrate the T-OAE here from Talghemt, and previously from Peniche (Boulila and Hinnov, 2017). Additional statistical tests were applied below to Peniche $d^{13}C$ data, but at the high-frequency band, to further argue for a shorter duration of the T-OAE. The objective of these additional tests is to compare the number of obliquity related $d^{13}C$ cycles between Peniche and Talghemt.

Furthermore, the Talghemt CIE is strongly correlatable to Peniche CIE. The two sections share similar general trends (Fig. 8), which is essential for the definition of CIE. Interestingly, a recent

estimate of the duration of the T-OAE at Peniche yields ~472 kyr (Boulila and Hinnov, 2017), which is again in excellent accord with the 400-500 kyr duration inferred from Talghemt and with the 300-500 kyr duration obtained from Sancerre (Boulila et al., 2014). The stratigraphic extent of Pl-To event is not easy to define because the onset and the end of the associated CIE do not show abrupt changes but rather progressive trends. Nevertheless, we propose a rough duration of 120 kyr based on our definition of the CIE (Fig. 7). Previous cyclostratigraphic estimates from Foum Tillicht section in the central High Atlas Basin, and Issouka section in the Middle Atlas Basin provided durations for the Pl-To CIE of respectively 0.18-0.27 Myr (Martinez et al., 2017), and 0.24 ±0.02 Myr (Ait-Itto et al., 2018).

The thickness of Talghemt section with respect to other sections in the Atlas of Morocco is relatively reduced. For instance, the Polymorphum ammonite zone interval is almost 30 m thick at Talghemt section. The same equivalent interval is almost 65 m thick at Amellago section (Bodin et al., 2010, 2016), and almost 40 m thick at Issouka section (Ait-Itto et al., 2018). The Issouka section was used for cyclostratigraphy to assess the duration of Polymorphum Zone at 1 ±0.08 Myr (Ait-Itto et al., 2018). Although the upper boundary of Polymorphum Zone is not biostratigraphically well defined at Talghemt, $d^{13}C$ correlation with other sections (Fig. 8 and Fig. S1) permits placement of this boundary at nearly 36 m stratigraphic position. Assuming this boundary, a duration of 0.925 Myr could be retrieved for the Polymorphum Zone at Talghemt, on the basis of the 405 kyr cyclostratigraphic timescale (Fig. 7). Thus, this duration is very close to the 1 ±0.08 Myr duration inferred from the relatively more expanded Issouka section (Ait-Itto et al., 2018). Accordingly, significant condensation or hiatus at Talghemt section is unlikely. The same study of Ait-Itto et al. (2018) claimed that the longer 900 kyr duration (e.g., Suan et al., 2008b) of the T-OAE is more appropriate than the shorter 300-500 kyr duration (e.g., Boulila et al., 2014), while their studied Issouka section does not record the T-OAE time interval. They further went to estimate ages for the base and end of T-OAE to draw conclusions on implications of these ages for LIP phases. Ait-Itto et al.'s (2018) main argument for a longer 900 kyr duration is that the hypothesis of a hiatus of ~700 kyr in the Polymorphum Zone and within the Pl-To transition (Boulila and Hinnov, 2017) is unlikely. They referred to $d^{13}C$ data (Pittet et al., 2014) as an indicator against this potential hiatus. However, Pittet et al. (2014) pointed out multiple sedimentary discontinuities at Peniche and elsewhere in the Lusitanian Basin, with the most important ones occurred near the Pl-To transition and in the Polymorphum Zone before or close to the onset of T-OAE. Correlation based on $d^{13}C$ data could point to possible hiatuses (Pittet et al., 2014), however, the cyclostratigraphic approach could, in addition, quantify their durations (Boulila and Hinnov, 2017). In Figure 9, we provide additiononal time-series analysis of Peniche $d^{13}C$ data to further argue for a shorter duration of the T-OAE, and for a potential hiatus in the Polymorphum Zone. A strong evidence for a possible hiatus in the Polymorphum Zone at Peniche comes from $d^{13}C$ correlation, together with comparison of the differential thickness among different parts between Talghemt and Peniche sections (Figs. 8A and 9). The total thickness of CIE at Peniche is ~24 m versus only ~18 m at Talghemt (Fig. 10A). This implies that sedimentation rate within the CIE at Peniche should be higher than at Talghemt. This result is supported by the wavelength of obliquity related spectral peak, which is ~1.4 m at Peniche (Kemp et al., 2011; Boulila and Hinnov, 2017), but only ~1 m at Talghemt (Fig. 4). Also, the T-OAE includes 15 to 17 $d^{13}C$ obliquity related cycles (maximal duration) at Peniche (Fig. 9), and 16 to 17 cycles (maximal duration) at Talghemt (Fig. 7). Boulila and Hinnov (2017) inferred only 13.5 to 14.5 obliquity cycles from $\%CaCO_3$ data at Peniche, however, they missed one cycle and a half in their counting (see their Fig. 5C). The interval from the base of CIE to the end of $\%CaCO_3$ signal encompasses 14 to 15 obliquity cycles, in addition to the extrapolated cycle in the uppermost part of CIE (to reach its end). Thus, the T-OAE should include 15 to 16 $\%CaCO_3$ obliquity related cycles, which is in accord with the 15 to 17 cycles from $d^{13}C$ data (Fig. 9). The close number of obliquity cycles within the T-OAE at Peniche and Talghemt sections provides strong evidence for the completeness of CIE in both sections.

In contrast, the interval from the Pl-To boundary till the onset of T-OAE is only ~7.5 m thick at Peniche versus ~28 m at Talghemt (see Fig. 8A, note that the two sections Talghemt and Peniche in Fig. 8A are reset to the same stratigraphic scale). Thus, such considerable difference in thickness along with time-series analysis (Figs. 7 and 9) further support the hypothesis of a significant hiatus of about 700 kyr in the Polymorphum Zone including the Pl-To transition.

In summary, the close duration of T-OAE obtained from Talghemt cyclostratigraphy (Section 2.2) and previous T-OAE cyclostratigraphies, especially from NW Europe (Boulila et al., 2014), hints at less influence of sedimentary hiatuses within the CIE. The Talghemt section is the first cyclostratigraphic record from the High Atlas of both Pl-To and T-OAE events, possibly owing to its specific sedimentary environment (Section 1.1). The duration of 300-500 kyr of the T-OAE is also supported by Ikeda et al. (2017, 2018) from deep-sea sedimentray successions in Japan. Finally, this shorter duration is compatible with carbon-cycle modeling of the magnitude of CIE (e.g., Beerling and

Brentnall, 2007; Them et al., 2017a), but also with numerical modeling of other geochemical cycles (e.g., Them et al., 2017a).

3.3. Obliquity dominance during the Pl-To and T-OAE events

The Pliensbachian-Toarcian (Pl-To) transition at Talghemt is lithologically marked by pronounced alternations of limestones and marls (Fig. 2). The 405 kyr tuning calibrates the mean thickness of these marl-limestone alternations to the obliquity cycle band (Figs. 4 and 5). The occurrence of strong obliquity cycles with weak precession cycles at the Pl-To transition was previously detected at Sancerre (Paris Basin) (Boulila and Hinnov, 2017). It has been postulated that significant paleoenvironmental and sea-level changes (from glacio-eustasy) may have been driven by obliquity, a hypothesis consistent with transient ice sheets at Pl-To transition (e. g., Hinnov and Park, 1999; Price, 1999; Hinnov et al., 2000; Cobianchi and Picotti 2001; Guex et al., 2001, 2016; Bailey et al. 2003; Morard et al. 2003; van de Schootbrugge et al. 2005; Suan et al. 2010; Guex, 2016).

In addition, the obliquity signal dominates the decreasing part of the T-OAE CIE (hereafter DP-CIE, see Boulila and Hinnov, 2017, for a review). There are seven or eight short-term $d^{13}C$ oscillations at Talghemt, calibrated to the obliquity cycle band (Fig. 10).

Six or seven $d^{13}C$ obliquity related oscillations within the DP-CIE are recorded in the supposedly more complete section at Sancerre (Fig. 10; Boulila and Hinnov, 2017). At Yorkshire, there are only four or five $d^{13}C$ oscillations implying a possible hiatus of one to three obliquity cycles (Kemp et al., 2011; Boulila and Hinnov, 2017). At Peniche, there are only five or six $d^{13}C$ obliquity cycles, depending on the selected onset of CIE. These five or six $d^{13}C$ obliquity cycles at Peniche end by a thick (~50 cm) turbidite level, which marks the base of the '*Plateau*'. Kemp et al. (2011) correlated the turbidte level to the aforementioned hiatus at Yorkshire, and suggested an erosional surface within the turbidite level at Peniche. This proposed hiatus should be minor and may not significantly affect the total duration of CIE since recent cyclostratigraphic reinterpretation of Peniche arrived at a duration similar to those inferred from other sites (Section 3.1). Furthermore, the DP-CIE at Peniche does not end at the turbidte level. The most prominent $d^{13}C$ obliquity-scale cycle could be observed immediately after the '*Plateau*', which is very similar to cycle number 7 at Talghemt (Fig. 10).

Although the Talghemt general CIE is strongly correlatable to Peniche CIE (Fig. 8), correlation at high-frequency obliquity $d^{13}C$ cycles is not evident between the two sections (Fig. 10) because there is a significant '*Plateau*' at Peniche versus a reduced '*Plateau*' or no '*Plateau*' at Talghemt (Fig. 8). Thus, the presence of the '*Plateau*' at Peniche makes the definition of the end of DP-CIE delicate (Boulila and Hinnov, 2017), hence the comparison of the number of recorded obliquity cycles within the DP-CIE, between Peniche and Talghemt sections, unmeaningful. Comparison of the number of obliquity cycles within the whole CIE shows, however, consistent results between the two sections (Section 3.2).

The presence of turbidite levels as well as the potential effects of diagenesis on $d^{13}C$ record at Talghemt could not be excluded (Section 3.1). The T-OAE cyclostratigraphic records that we have today come either from condensed sections in NW Europe or from sections with relatively higher sedimentation rates, but with frequent turbidite levels, in the Lusitanian and High Atlas basins.

In summary, the Talghemt section shows an additional record of the obliquity within the DP-CIE (Fig. 10). The expression of the obliquity during the T-OAE was ascribed to its modulating effect on the carbon cycle by lengthened continental plant growing season (organic phenology, e.g., Reyes-Fox et al., 2014), beneath substantially enhanced greenhouse CO_2 and the resulting global warming from volcanism (Boulila and Hinnov, 2017). There is increasing evidence for the impact of T-OAE global warming and the released CO_2 on continental paleoenvironments such as the acceleration of weathering rates and intensification of the hydrological cycle (e.g., Cohen et al., 2004; Bodin et al. 2011; Brazier et al., 2015; Montero-Serrano et al. 2015; Boulila and Hinnov, 2017; Them et al., 2017a; Izumi et al., 2018). Other scenarios to explain obliquity paced $d^{13}C$ cycles during the T-OAE are listed in the Section below.

3.4. Evidence for carbon-reservoir change across the T-OAE and paleoenvironmental implications

In this study we show the first direct evidence for change in C reservoir during the T-OAE. This change in C reservoir is expressed as a shift in the phase between $\%CaCO_3$ and $d^{13}C$ orbitally related cyclicities (Fig. 7). Within the T-OAE, the $\%CaCO_3$ and $d^{13}C$ cycles are sometimes phase shifted, but sometimes in opposite phase. Outside the T-OAE, cycles are mostly in coherent in-phase (Fig. 7). This phase change could also be observed at Peniche, where high-resolution $\%CaCO_3$ and $d^{13}C$ data before and within the T-OAE allows such finding. At Peniche, the onset of CIE marks a

phase change from in-phase to opposite-phase between %$CaCO_3$ and $d^{13}C$ obliquity related cycles (see figure 9 of Boulila and Hinnov, 2017).

The negative CIE of the Pl-To event has a shorter duration (~120 kyr) than the negative CIE associated to the T-OAE (~400 to ~500 kyr) (Fig. 7). Moreover, %$CaCO_3$ and $d^{13}C$ cycles are in phase during the Pl-To event, but phase shifted during the T-OAE. This may imply different driving mechanisms on the carbon cycle perturbation during the two events. Interestingly, a recent study suggests different paleoenvironmental implications of the two events, both linked to the Karoo-Ferrar magmatic activity but in two distinct phases (Guex et al., 2016).

The Pl-To event may have been caused by sulfur release from plume-cratonic lithosphere interaction (Guex et al., 2016). Such sulfur release, with an estimated flux of 90 Mt/yr and lasting ~120 kyr (our estimate, Fig. 7), might explain severe climatic cooling, transient ice sheets and glacioeustatic fall (e.g., Guex et al., 2001; Suan et al., 2010; Dera et al., 2011). Such paleoenvironmental conditions may be responsible for the initiation of the main phase of mass extinction, associated with the Pl-To event. Thus, the predominance of the obliquity at the Pl-To transition may reflect its role on transient ice sheets (Section 3.3).

During the T-OAE, a second Karoo-Ferrar magmatic phase, which may be characterized by flood basalt volcanism, CH_4 thermogenic release by dyke and sill emplacement into organic matter rich sedimentary sequences, and huge CO_2 degassing (Guex et al., 2016). Thus, the amplification of the obliquity at the T-OAE may have impacted on the carbon cycle via volcanically released greenhouse gases (see different scenarios below). Substantial release of CO_2 and widespread oceanic anoxia (e.g., Jenkyns, 1988, 2010; Ikeda et al., 2018; Them et al., 2018) were likely responsible for the second biological crisis of the T-OAE affecting mainly benthic fauna and less nectonic fauna (e.g., Bartolini et al., 1992; Morard et al., 2003; Guex et al., 2016). Although calcareous phytoplankton did not suffer from a major extinction crisis, a decreased nannofossil $CaCO_3$ flux to the bottom seawater, a succession of calcareous nannofossil extinction events as well as a reduction in size of the major pelagic carbonate producers (*Schizosphaerella*) have been observed (Tremolada et al., 2005; Mattioli et al., 2008, 2009; Suan et al., 2008a; Clémence et al., 2015). This concurs with a diminished CO_2 biological pump efficacy and with an increased volcanic CO_2 emission (Gardin and Bartolini 2016).

From the above discussion, the resulting forcing processes from volcanism during the T-OAE and Pl-To events may not be the same (Guex et al., 2016), and could be supported here by the different phase relationship between $CaCO_3$ and $d^{13}C$ obliquity related cycles.

Despite the general decrease of %$CaCO_3$ values at the initiation part of T-OAE at Talghemt (Fig. 2), but also at other T-OAE equivalent sections (e.g., Peniche, see figure 5 of Boulila and Hinnov, 2017), we note high-amplitude oscillations at the scale of obliquity cycles, especially within the DP-CIE. These high-amplitude %$CaCO_3$ variations could result from strong climate response to substantially released greenhouse gases (e.g., Boulila and Hinnov, 2017; Them et al., 2017b), likely CH_4 thermogenic release by dyke and sill emplacement into organic matter rich sedimentary sequences (e.g., McElwain et al., 2005; Svensen et al., 2007, 2012; Sell et al., 2014). Amplification of obliquity forced insolation may reflect highly contrasted seasonality during the general warming trend of T-OAE (e.g., Hermoso et al., 2012 their figure 1). Higher temperatures and more intense precipitation (e.g., Dera and Donnadieu, 2012) would enhance continental weathering and intensify the hydrological cycle (e.g., Cohen et al., 2004; Bodin et al. 2011; Kemp and Izumi, 2014; Brazier et al., 2015; Krencker et al., 2015; Montero-Serrano et al. 2015; Boulila and Hinnov, 2017; Them et al., 2017a; Han et al., 2018; Izumi et al., 2018; Xu et al., 2018). In addition, the T-OAE interval was marked by a global sea-level rise (e.g., Hallam et al., 1981 ; Haq et al., 1987), that caused drowning carbonate platforms, leading to extinction of carbonate-platform depositional system in the High Atlas Basin (e.g., Bassoullet and Baudin, 1994; Blomeier and Reijmer, 1999; Wilmsen and Neuweiler, 2008). Thus, the pelagic carbonate factory during the early Toarcian may be the principal source of carbonate production in the Talghemt site. Accordingly, we suggest that the phase change between %$CaCO_3$ and $d^{13}C$ obliquity cycles was related to a disturbance in the carbonate production in the pelagic environment. Several scenarios could be evoked to explain this phase change at the T-OAE, such as obliquity modulated: (1) ocean circulation leading to ventillation cycles, (2) formation of upwelling cells, (3) inputs of methane from clathrate reservoirs (Hesselbo et al., 2000; Kemp et al., 2005 ; Hesselbo and Pienkowski, 2011) or from terrestrial methanogenesis (Them et al., 2017b), and (4) ocean acidification counterbalanced by continental weathering.

The first scenario of obliquity paced ventillation cycles could not be applied to the High Atlas Basin because there aren't strong arguments for anoxia in this basin, or at least at the Talghemt site (Bodin et al., 2011). The potential of obliquity to drive mass ocean circulation has been suggested for glacial epochs (e.g., Caley et al., 2011), and the early Cretaceous OAE2 (Meyers et al., 2012).

The second possible scenario of upwellings was previously suggested for the T-OAE (e.g., Schouten et al., 2000; McArthur et al., 2008). The formation of upwelling cells during the global T-OAE warming is likely. A severe warming would enhance atmospheric circulation and intensify wind surface, and the creation of upwelling zones, which would bring lower $d^{13}C$ values to seawater surfaces. Thus, such mass recycling in the seawater column may explain the observed phase change during the T-OAE. Nevertheless, the hypothesis of effect of upwellings on $d^{13}C$ would limit the geographic extent of CIE, but also its global magnitude (e.g., Suan et al., 2011).

The third possible scenario of methane release from clathrate reservoirs is unlikely because the dominant symmetric nature of obliquity related $d^{13}C$ cycles and the longer duration (240 kyr) over which the cycles spanned (Boulila and Hinnov, 2017). The problem with invoking successive massive releases of CH_4 from gas hydrate systems (Hesselbo et al., 2000; Kemp et al., 2005) revolves around carbon total mass recharge. Large amounts of CH_4 would have to reform relatively quickly to (partly) replenish carbon loss following an injection (Dickens, 2011). However, obliquity paced terrestrial methanogenesis (Them et al., 2017b) remains a potential process because the production of CH_4 from terrestrial environments (e.g. wetlands, lakes, and soils) could be orbitally paced.

The fourth scenario of impact of ocean acidification on biocalcification followed by ocean alkalinity recovery was also suggested by Trecalli et al. (2012) from the Apennine carbonate platform in Italy. A dramatic crisis of hypercalcifying organisms in carbonate platform environments (e.g., Lithiotis bivalves), as well as of carbonate-saturation sensitive aragonitic Dasycladalean algae and corals across the T-OAE has been related to ocean acidification (Trecalli et al., 2012). Also, a severe disturbance in heavily calcifying organisms in pelagic realms (e.g. *Schizospherella*) was also documented (e.g., Erba, 2004; Mattioli et al., 2004; Tremolada et al., 2005; Suan et al., 2008a). Massive injection of volcanic CO_2 into the atmosphre-ocean system would increase ocean acidification, decrease biocalcification, and may cause the inversion phase between $d^{13}C$ and $CaCO_3$ variations. However, the cyclic nature of $d^{13}C$ and $CaCO_3$ within the T-OAE would recall another antagonist process to ocean acidification, to generate such obliquity related cycles. Continental rock weathering has generally been posited to buffer the excess in CO_2 in ocean by bringing more alkalinity to the ocean by rivers. This would counterbalance ocean acidity by keeping seawater surface supersaturated, hence lead to burial of $CaCO_3$. Nevertheless, the two above processes could occur at different timescales, 1 kyr to tens of 10 kyr for ocean acidification, and 1 kyr to 100 kyr for the weathering process (e.g., Panchuk et al., 2008; Zeebe et al., 2009). These two timescales fall into the obliquity time variations. Thus, obliquity forcing could act as a modulator of these two processes, without requiring the symmetric vs asymmetric nature of $d^{13}C$ and $CaCO_3$ cyclic variations (Boulila and Hinnov, 2017). During protracted volcanic activity of the Karoo-Ferrar LIP (Courtillot et al., 1999; Palfy and Smith, 2000; Svensen et al., 2007, 2012; Jourdan et al., 2008; Sell et al., 2014; Burgess et al., 2015; Moulin et al., 2017), higher levels of atmospheric pCO_2 may have caused the general trend of CIE, while obliquity forcing may control $d^{13}C$ swings by modulating the intensity of relative injection of CO_2 into the ocean, counterbalanced by the weathering process. This last scenario is plausible, however, it needs more investigation in order to approach the couple process of ocean acidification and alkalinity recovery in the expression of obliquity-scale cycles.

4. Conclusions

High-resolution $d^{13}C$ data of the early Toarcian Talghemt sedimentary section (High Atlas, Morocco) captures the two negative carbon isotope excursions (CIE) of T-OAE and Pliensbachian-Toarcian (Pl-To) transition. The Talghemt $d^{13}C$ data strongly correlates to Peniche (Portugal) $d^{13}C$ reference data, and to other key $d^{13}C$ records from the NW European basins.

A cyclostratigraphic study based on high-resolution carbonate content (%$CaCO_3$) and $d^{13}C$ data of Talghemt section shows evidence for astronomical forcing by the precession, obliquity, short eccentricity (~110 kyr) and the stable 405 kyr eccentricity. Orbital calibration of the early Toarcian based on the 405 kyr stable period yields a duration of the T-OAE ranging from 400 to 500 kyr, supporting previous estimates (300 to 500 kyr) from Sancerre Core (Paris Basin).

In addition, the 405 kyr orbital tuning of the Talghemt section calibrated the principal obliquity period O1 to a ~30 kyr period, which is significantly shorter than the theoretically predicted 35 kyr period in the La2004 astronomical model. This implies a possible early Jurassic tidal dissipation factor of the Earth different to that theoretically predicted.

Finally, the 405 kyr tuning calibrates the high-frequency $d^{13}C$ cyclicities at the Pl-To transition and those at the decreasing part of CIE associated to T-OAE to the obliquity cycle band. We suggest that the dominance of the obliquity at the Pl-To transition may reflect its role on transient ice sheets, while the amplification of the obliquity at the T-OAE may have rather impact on the carbon cycle via

volcanically released greenhouse gases. This hypothesis is supported by a significant phase change between $d^{13}C$ and $\%CaCO_3$ cycles at the T-OAE, but not at the Pl-To transition.

Acknowledgements

This work was supported by the "Institut National des Sciences de l'Univers–CNRS" (*INSU-SYSTER Grant 2015* to S. Boulila and B. Galbrun). We thank Michael Brussaferi for the first analyses obtained as part of his master degree. We warmly thank Ravi Dalliah (CR2P MNHN) for significant help in carbonate content measurements, as well as Denis Fiorillo (SSMIM MNHN) for carbon isotope analyses. S.B. thank Jacques Laskar for helpful discussions, especially about the tidal-dissipation factor. We thank the Editor Prof. Zhengtang Guo, Dr. Andrew Caruthers, and an anonymous reviewer for vey helpful constructive comments.

References

Ait-Itto, F-Z., Martinez, M., Price, G.D., Ait-Addi, A., 2018. Synchronization of the astronomical time scales in the Early Toarcian: A link between anoxia, carbon-cycle perturbation, mass extinction and volcanism. Earth Planet. Sci. Lett., 493, 1–11.

Bailey, T.R., Rosenthal, Y., McArthur, J.M., van de Schootbrugge, B., Thirlwall, M.F., 2003. Paleoceanographic changes of the late Pliensbachian-early Toarcian interval: A possible link to the genesis of an oceanic anoxic event. Earth Planet. Sci. Lett. 212, 307–320.

Bartolini, A., Nocchi, M., Baldanza, A., Parisi, G., 1992. In Studies in benthic Foraminifera. Proceedings of the Fourth International Symposium on Benthic Foraminifera, Sendai, 1990. (eds Y. Takayanagi & T. Saito) 323–338 (Tokai University Press, 1992).

Bassoullet, J.P., Baudin, F., 1994. Le Toarcien inférieur : une épisode de crise dans les bassins et sur les plate-formes carbonatées de l'Europe du Nord-Ouest et de la Téthys. Geobios Mem. Spec. 17, 645–654.

Beerling, D.J., Brentnall, S.J., 2007. Numerical evaluation of mechanisms driving Early Jurassic changes in global carbon cycling. Geology 5, 247–250.

Blomeier, D.P.G., Reijmer, J.J.G.,1999. Drowning of a Lower Jurassic carbonate platform: Jbel Bou Dahar, High Atlas, Morocco. Facies 41,81–110.

Bodin, S., Fröhlich, Boutib, L., Lahsini, S., Redfern, J., 2011. Early Toarcian source-rock potential in the central High Atlas Basin (Central Morocco): regional distribution and depositional model. J. Petrol. Geol. 34(4), 345–364.

Bodin, S., Krencker, F.-N., Kothe, T., Hoffmann, R., Mattioli, E., Heimhofer, U., Kabiri, L., 2016. Perturbation of the carbon cycle during the late Pliensbachian – Early Toarcian: New insight from high-resolution carbon isotope records in Morocco. Journal of African Earth Sciences 116, 89–104.

Bodin, S., Mattioli, E., Fröhlich, S., Marshall, J.D., Boutib, L., Lahsini, S., Redfern, J., 2010. Toarcian carbon isotope shifts and nutrient changes from the Northern margin of Gondwana (High Atlas, Morocco, Jurassic): palaeoenvironmental implications. Palaeogeogr. Palaeoclimatol. Palaeoecol. 297, 377–390.

Boulila, S., Galbrun, B., Huret, E., Hinnov, L.A., Rouget, I., Gardin, S., Bartolini, A., 2014. Astronomical calibration of the Toarcian Stage: implications for sequence stratigraphy and duration of the early Toarcian OAE. Earth Planet. Sci. Lett. 386, 98–111.

Boulila, S., Hinnov, L.A., 2015. Comment on "Chronology of the Early Toarcian environmental crisis in the Lorraine Sub-Basin (NE Paris Basin)" by W. Ruebsam, P. Münzberger, and L. Schwark [Earth and Planetary Science Letters 404 (2014) 273–282]. Earth Planet. Sci. Lett. 416, 143–146.

Boulila, S., Hinnov, L.A., 2017. A review of tempo and scale of the early Jurassic Toarcian OAE: implications for carbon cycle and sea level variations. Newsletters on Stratigraphy 50/4, 363–389.

Brazier, J.-M., Suan, G., Tacail, T., Simon, L., Martin, J.E., Mattioli, E., Balter, V., 2015. Calcium isotope evidence for dramatic increase of continental weathering during the Toarcian oceanic anoxic event (Early Jurassic). Earth Planet. Sci. Lett. 411, 164–176.

Burgess, S.D., Bowring, S.A., Fleming, T.H., Elliot, D.H., 2015. High-precision geochronology links the Ferrar large igneous province with early-Jurassic ocean anoxia and biotic crisis. Earth Planet. Sci. Lett. 415, 90–99.

Caley, T., Kim, J.-H., Malaizé, B., Giraudeau, J., Laepple, T., Caillon, N., Charlier, K., Rebaubier, H., Rossignol, L., Castaneda, I.S., Schouten, S., Sinninghe Damsté, J.S., 2011. High-latitude obliquity as a dominant forcing in the Agulhas current system. Clim. Past, 7, 1285–1296.

Caruthers, A.H., Smith, P.L., Gröcke, D.R., 2013. The Pliensbachian–Toarcian (Early Jurassic) extinction, a global multi-phased event. Palaeogeogr. Palaeoclimatol. Palaeoecol. 386, 104–118, doi: 10.1016/j.palaeo.2013.05.010.

Caruthers, A.H., Smith, P.L., Gröcke, D.R., 2014. The Pliensbachian–Toarcian (Early Jurassic) extinction: A North American perspective. Geological Society of America Special Papers 505, 225-243, doi:10.1130/2014.2505(11).
Clémence, M-E., Gardin, S., Bartolini, A., 2015. New insights in the pattern and timing of the Early Jurassic calcareous nannofossil crisis. Palaeogeogr. Palaeoclimatol. Palaeoecol. 427, 100–108.
Cleveland, W.S., 1979. Robust locally weighted regression and smoothing scatter plots. J. Am. Stat. Assoc. 74, 829–836.
Cobianchi, M., Picotti, V., 2001. Sedimentary and biological response to sea-level and paleoceanographic changes of a Lower–Middle Jurassic Tethyan platform margin (Southern Alps, Italy). Palaeogeogr. Palaeoclimatol. Palaeoecol. 169, 219–244.
Cohen, A.S., and Coe, A.L., 2007. The impact of the Central Atlantic Magmatic Province on climate and on the Sr- and Os-isotope evolution of seawater. Palaeogeogr. Palaeoclimatol. Palaeoecol. 244, 374–390.
Cohen, A.S., Coe, A.L., Harding, S.M., Schwark, L., 2004. Osmium isotope evidence for the regulation of atmospheric CO2 by continental weathering. Geology 32, 157–160.
Courtillot, V., Jaupert, C., Manighetti, I., Tapponier, P., Besse, J., 1999. On Causal links between flood basalts and continental break-up. Earth Planetary Science Letters 166, 177–195.
De Kaenel, E., Bergen James, A., von Salis Perch Nielsen, K., 1996. Jurassic calcareous nannofossil biostratigraphy of Western Europe; compilation of recent studies and calibration of bioevents. Bulletin de la Societe Géologique de France 167, 15–28.
Dera, G., Brigaud, B., Monna, F., Laffont, R., Pucéat, E., Deconinck, J.-F., Pellenard, P., Joachimski, M.M., Durlet, C., 2011. Climatic ups and downs in disturbed Jurassic world. Geology 39, 215–218.
Dera, G.D., Donnadieu, Y., 2012. Modeling evidence for global warming, Arctic seawater freshening, and sluggish ocean circulation during the Early Toarcian anoxic event. Paleoceanography 27, PA2211.
Dera, G., Neige, P., Dommergues, J.L., Brayard, A., 2011. Ammonite paleobiogeography during the Pliensbachian-Toarcian crisis (Early Jurassic) reflecting paleoclimate, eustasy, and extinctions. Global and Planetary Change 78, 92–105.
Dera, G., Neige, P., Dommergues, J.-L., Fara, E., Laffont, R., Pellenard, P., 2010. High-resolution dynamics of Early Jurassic marine extinctions: the case of Pliensbachian–Toarcian ammonites (Cephalopoda). Journal of the Geological Society, London 167, 21–33, doi: 10.1144/0016-76492009-068.
Dera, G., Pellenard, P., Niege, P., Deconinck, J.-F., Puceat, E., Dommergues, J.-L., 2009. Distribution of clay minerals in Early Jurassic peritethyan seas: Palaeoclimatic significance inferred from multiproxy comparisons. Palaeogeogr. Palaeoclimatol. Palaeoecol. 271, 39–51.
Dickens, G.R., 2011. Down the rabbit hole: toward appropriate discussion of methane release from gas hydrate systems during the Paleocene-Eocene thermal maximum and other past hyperthermal events. Clim. Past 7, 831–846, doi:10.5194/cp-7-831-2011.
Duarte, L.V., 1998. Clay minerals and geochemical evolution in the Toarcian–lower Aalenian of the lusitanian basin (Portugal). Cuad. Geol. Ibérica 24, 69–98.
Dubar, G., 1932. Le Lias et le Jurassique de la Haute Moulouya et du Haut-Atlas (Sud et Sud-Est de Midelt). Bulletin de la Société géologique de France (5), 2, 573–594.
El Hariri, K., 1990. Etude stratigraphique et paléontologique du Lias moyen – Dogger basal des régions de Bou-Ouchène, Tizi n'Zou et Talghemt (Haut-Atlas central). Thèse 3e cycle, Univ. Cadi Ayyad Marrakech, 180p.
El Kamar, A., Boutakiout, M., Elmi, S., Sadki, D., Ruget, C., 1997. Foraminifères et ostracodes du Lias supérieur et du Bajocien de la Ride de Talghemt (Haut- Atlas central, Maroc). Bulletin de l'Institut Scientifique, Rabat 21, 31-41.
Elmi, S., 2006. Pliensbachian/Toarcian boundary: the proposed GSSP of Peniche (Portugal). Volumina Jurassica, Volumen IV, 5–16.
Erba, E., 2006. The first 150 million years history of calcareous nannoplankton; biosphere-geosphere interactions. Palaeogeogr. Palaeoclimatol. Palaeoecol. 232, 237–250.
Gardin, S., Bartolini, A., 2016. Reply to the comment on "New insights in the pattern and timing of the Early Jurassic calcareous nannofossil crisis" by M. Clémence, S. Gardin, S. A. Bartolini [*Palaeogeography Palaeoclimatology Palaeoecology 427* (2015) 100–108]. Palaeogeogr. Palaeoclimatol. Palaeoecol. 427, 100–108.
Gill, B.C., Lyons, T.W., Jenkyns, C., 2011. A global perturbation to the sulfur cycle during the Toarcian oceanic anoxic event. Earth Planet. Sci. Lett. 312(3–4), 484–496.
Gómez, J.J., Goy, A., Canales, M.L., 2008. Seawater temperature and carbon isotope variations in belemnites linked to mass extinction during the Toarcian (Early Jurassic) in Central and Northern Spain. Comparison with other European sections. Palaeogeogr. Palaeoclimatol. Palaeoecol. 258, 28–

58.
Guex, J., 2016. Retrograde evolution during major extinctions crises. Springer Cham Heidelberg New York Dordrecht London. 77p, doi: 10.1007/978-3-319-27917-6.
Guex, J., Morard, A., Bartolini, A., Morettini, E., 2001. Découverte d'une importante lacune stratigraphique à la limite Domérien-Toarcien: implications paléocéanographiques. Bull. Soc. Vaud. Sci. Nat. 345, 277–284.
Guex, J., Pilet, S., Müntener, O., Bartolini, A., Spangenberg, J., Schoene, B., Sell, B., Schalteggers, U., 2016. Thermal erosion of cratonic lithosphere as a potential trigger for mass-extinction. Scientific Reports 6:23168. doi: 10.1038/srep23168.
Hallam, A., 1981. A revised sea-level curve for the early Jurassic. J. Geol. Soc. 138, 738–743.
Haq, B.U., Hardenbol, J., Vail, P.R., 1987. Chronology of fluctuating sea levels since the Triassic. Science 235, 1156–1167.
Hana, Z., Hua, X., Kemp, D.B., Lia, J., 2018. Carbonate-platform response to the Toarcian Oceanic Anoxic Event in the southern hemisphere: Implications for climatic change and biotic platform demise. Earth Planet. Sci. Lett. 489, 59–71.
Harries, P.J., Little, C.T.S., 1999. The early Toarcian (Early Jurassic) and the Cenomanian-Turonian (Late Cretaceous) mass extinctions: similarities and contrasts. Palaeogeogr. Palaeoclimatol. Palaeoecol. 154, 39–-66.
Hermoso, M., Le Callonnec, L., Minoletti, F., Renard, M., Hesselbo, S.P., 2009. Expression of the Early Toarcian carbon-isotope negative excursion in separated microfractions (Jurassic, Paris Basin). Earth Planet. Sci. Lett. 277, 194– 203.
Hermoso, M., Minoletti, F., Pellenard, P., 2013. Black shale deposition during Toarcian super-greenhouse driven by sea level. Clim. Past 9, 2703–2712.
Hermoso, M., Minoletti, F., Rickaby, R.E.M., Hesselbo, S.P., Baudin, F., Jenkyns, H.C., 2012. Dynamics of a stepped carbon-isotope excursion: Ultra high-resolution study of Early Toarcian environmental change. Earth Planet. Sci. Lett. 319–320, 45–54.
Hesselbo, S.P., Gröcke, D.R., Jenkyns, H.C., Bjerrum, C.J., Farrimond, P., Morgans Bell, H.S., Green, O.R., 2000. Massive dissociation of gas hydrate during a Jurassic oceanic anoxic event. Nature 406, 392–395.
Hesselbo, S.P., Jenkyns, H.C., Duarte, L.V., Oliveira L.C.V., 2007. Carbon-isotope record of the Early Jurassic (Toarcian) Oceanic Anoxic Event from fossil wood and marine carbonate (Lusitanian Basin, Portugal). Earth Planet. Sci. Lett. 253, 455–470.
Hesselbo, S.P., Pienkowski, G., 2011. Stepwise atmospheric carbon-isotope excursion during the Toarcian Oceanic Anoxic Event (Early Jurassic, Polish Basin). Earth Planet. Sci. Lett. 301, 365–372.
Hinnov, L.A., 2013. Cyclostratigraphy and its revolutionizing applications in the earth and planetary sciences. GSA Bulletin 125, no. 11/12, 1703–1734.
Hinnov, L.A., Park, J., 1999. Strategies for assessing Early-Middle (Pliensbachian-Aalenian) Jurassic cyclochronologies, in Shackleton, N.J., Mc Cave, I.N., and Weedon, G.P., eds*., A Discussion: Astronomical (Milankovitch) Calibration of the Geological Timescale, Philosophical Transactions of the Royal Society, London, Series A*, 357, pp. 1831–1859.
Hinnov, L.A., Park, J., Erba, E., 2000. Lower-Middle Jurassic rhythmites from the Lombard Basin, Italy: a record of orbitally forced carbonate cycles modulated by secular environmental changes in West Tethys, in, R.L. Hall and P.L. Smith, eds., *Advances in Jurassic Research 2000*, Trans Tech Publications, pp. 437-454.
Huang, C., Hesselbo, S.P., 2014. Pacing of the Toarcian Oceanic Anoxic Event (Early Jurassic) from astronomical correlation of marine sections. Gondwana Res. 25, 1348–1356.
Huang, C., Hinnov, L.A., Fischer, A.G., Grippo, A., Herbert, T., 2010. Astronomical tuning of the Aptian Stage from Italian reference sections. Geology 38, 899–902.
Ikeda, M., Hori, R.S., Ikehara, M., Miyashita, R., Chino, M., Yamada, K., 2018. Carbon cycle dynamics linked with Karoo-Ferrar volcanism and astronomical cycles during Pliensbachian-Toarcian (Early Jurassic). Global and Planetary Change 170, 163–171.
Ikeda, M., Tada, R., Ozaki, K., 2017. Astronomical pacing of the global silica cycle recorded in Mesozoic bedded cherts. Nat. Commun. 8, 15532.
Izumi, K., Kemp, D.b., Itamiya, S., Inui, M., 2018. Sedimentary evidence for enhanced hydrological cycling in response to rapid carbon release during the early Toarcian oceanic anoxic event. Earth Planet. Sci. Lett. 481, 162–170.
Jenkyns, H.C., 1988. The early Toarcian (Jurassic) anoxic event: stratigraphic, sedimentary and geochemical evidence. Am. J. Sci. 288, 101–151.
Jenkyns, H.C., 2010. Geochemistry of oceanic anoxic events, Geochem. Geophys. Geosyst. 11, Q03004, doi:10.1029/2009GC002788.

Jourdan, F., Féraud, G., Bertrand, H., Watkeys, M.K., Renne, P.R., 2008. The 40Ar/39Ar ages of the sill complex of the Karoo large igneous province: implications for the Pliensbachian–Toarcian climate change. Geochem. Geophys. Geosyst. 9, Q06009. doi:10.1029/2008GC001994.

Kemp, D.B., Coe A.L., Cohen, A.S., Schwark, L., 2005. Astronomical pacing of methane release in the Early Jurassic period. Nature 437, 396–399.

Kemp, D.B., Coe, A.L., Cohen, A.S., Weedon, G.P., 2011. Astronomical forcing and chronology of the early Toarcian (Early Jurassic) Oceanic Anoxic Event in Yorkshire, UK, Paleoceanography 26, PA4210, doi:10.1029/2011PA002122.

Kemp, D.B., Izumi, K., 2014. Multiproxy geochemical analysis of a Panthalassic margin record of the early Toarcian oceanic anoxic event (Toyora area, Japan). Palaeogeogr. Palaeoclimatol. Palaeoecol. 414, 332–341.

Krencker, F.-N., Bodin, S., Suan, G., Heimhofer, U., Kabiri, L., Immenhauser, A., 2015. Toarcian extreme warmth led to tropical cyclone intensification. Earth Planet. Sci. Lett. 425, 120–130.

Laskar, J., Robutel, P., Joutel, F., Gastineau, M., Correia, A.C.M., Levrard, B., 2004. A long-term numerical solution for the insolution quantities of the Earth. Astron. Astrophys. 428, 261–285.

Macchioni, F., Cecca, F., 2002. Biodiversity and biogeography of middle–late liassic ammonoids: implications for the Early Toarcian mass extinction. Geobios 35, 150–164.

Mann, M.E., Lees, J.M., 1996. Robust estimation of background noise and signal detection in climatic time series. Clim. Change 33, 409–445.

Martinez, M., Krencker, F.-N., Mattioli, E., Bodin, S., 2017. Orbital chronology of the Pliensbachian – Toarcian transition from the Central High Atlas Basin (Morocco). Newsletters on Stratigraphy 50, 47–69.

Mattioli, E., Erba, E., 1999. Synthesis of calcareous nannofossil events in Tethyan Lower and Middle Jurassic successions. Rivista Italiana di Paleontologia e Stratigrafia 105, 343–376.

Mattioli, E., Pittet, B., Suan, G., Mailliot, S., 2008. Calcareous nannoplankton changes across the early Toarcian oceanic anoxic event in the western Tethys. Paleoceanography 23, PA3208. doi:10.1029/2007PA001435.

Mattioli, E., Pittet, B., Petitpierre, L., Mailliot, S., 2009. Dramatic decrease of pelagic carbonate production by nannoplankton across the Early Toarcian anoxic event (TOAE). Glob. Planet. Chang. 65 (3–4), 134–145.

McArthur, J.M., Algeo, T.J., van de Schootbrugge, B., Li, Q., Howarth, R.J., 2008. Basinal restriction, black shales, Re–Os dating, and the Early Toarcian (Jurassic) oceanic anoxic event. Paleoceanography 23, PA4217.

McArthur, J.M., Donovan, D.T., Thirlwall, M.F., Fouke, B.W., Mattey, D., 2000. Strontium isotope profile of the early Toarcian (Jurassic) oceanic anoxic event, the duration of ammonite biozones, and belemnite palaeotemperatures. Earth Planet. Sci. Lett. 179, 269–285.

McElwain, J.C., Wade-Murphy, J., Hesselbo, S.P., 2005. Changes in carbon dioxide during an anoxic event linked to intrusion of Gondwana coals. Nature 435, 479–482

Merino-Tomé, O., Porta, G.D., Kenter, J.A.M., Verwer, K., Harris, P.M., Adams, E.W., Playton, T., Corrochano, D., 2012. Sequence development in an isolated carbonate platform (Lower Jurassic, Djebel Bou Dahar, High Atlas, Morocco): influence of tectonics, eustacy and carbonate production. Sedimentology 59, 118–155.

Meyers, S.R., Sageman, B.B., Arthur, M.A., 2012. Obliquity forcing of organic matter accumulation during Oceanic Anoxic Event 2. Paleoceanography 27, PA3212, doi: 10.1029/2012PA002286.

Montero-Serrano, J-C., Föllmi, K.B., Adatte, T., Spangenberg, J.E., Tribovillard, N., Fantasia, A., Suan, G., 2015. Continental weathering and redox conditions during the early Toarcian Oceanic Anoxic Event in the northwestern Tethys: Insight from the Posidonia Shale section in the Swiss Jura Mountains. Palaeogeogr. Palaeoclim. Palaeoecol. 429, 83–99.

Morard, A., Guex, J., Bartolini, A., Morettini, E., de Wever, P., 2003. A new scenario for the Domerian–Toarcian transition. Bull. Soc. Géol. Fr. 174(4), 351–356.

Moulin, M., Fluteau, F., Courtillot, V., Marsh, J., Delpech, G., Quidelleur, X., Gérard, M., 2017. Eruptive history of the Karoo lava flows and their impact on early Jurassic environmental change. J. Geophys. Res. Solid Earth 122, doi:10.1002/2016JB013354.

Paillard, D., Labeyrie, L., Yiou, P., 1996. Macintosch program performs timeseries analysis. Eos 77, 379.

Palfy, J., Smith, P.L., 2000. Synchrony between Early Jurassic extinction, oceanic anoxic event, and the Karoo-Ferrar flood basalt volcanism. Geology 28, 747–750.

Panchuk, K., Ridgwell, A., Kump, L.R., 2008. Sedimentary response to the Paleocene-Eocene Thermal Maximum carbon release: A model-data comparison. Geology 36, 315–318.

Pittet, B., Suan, G., Lenoir, F., Duarte, L.V., Mattioli, E., 2014. Carbon isotope evidence for sedimentary discontinuities in the lower Toarcian of the Lusitanian Basin (Portugal): Sea level change at the onset

of the Oceanic Anoxic Event. Sedimentary Geology 303, 1–14.
Price, G.D., 1999. The evidence and implications of polar ice during the Mesozoic. Earth Science Reviews 48, 183–210.
Reyes-Fox, M., Steltzer, H., Trlica, M. J., McMaster, G. S., Andales, A. A., LeCain, D. R., Morgan, J. A., 2014. Elevated CO2 further lengthens growing season under warming conditions. Nature 510, 259-261.
Rocha et al., 2016. Base of the Toarcian Stage of the Lower Jurassic defined by the Global Boundary Stratotype Section and Point (GSSP) at the Peniche section (Portugal). Episodes 39, no. 3, 460–481.
Ruebsam, W., Münzberger, P., Schwark, L., 2014. Chronology of the Early Toarcian environmental crisis in the Lorraine Sub-Basin (NE Paris Basin). Earth Planet. Sci. Lett., 404, 273–282.
Sadki, D., 1996. Le haut-Atlas Central (Maroc): Stratigraphie et paléontologie du Lias supérieur et du Dogger inférieur, dynamique du bassin et des peuplements. Docum. Lab. Géol. Lyon, n° 142, 245 p., 50 fig., 10 pl.
Sadki, D., Elmi, S., Amhoud, H., 1999. Les formations jurassiques du Haut-Atlas central marocain : corrélations et évolution géodynamique. *1er Colloque national sur le Jurassique marocain*, Rabat. Moroccain Association of Petroleum Geologists, 122–123.
Schouten, S., Van Kaam-Peters, H.M.E., Rijpstra, W.E.C., Schoell, M., Sinninghe Damste, J.S., 2000. Effects of an Oceanic Anoxic Event on the stable carbon isotopic composition of early Toarcian carbon. Am. J. Sci. 300, 1–22.
Sell, B., Ovtcharova, M., Guex, J., Bartolini, A., Jourdan, F., Spangenberg, J.E., Vicente, J. C., Schaltegger, U., 2014. Evaluating the temporal link between the Karoo LIP and climatic biologic events of the Toarcian Stage with high-precision U–Pb geochronology. Earth Planet. Sci. Lett. 408, 48–56.
Suan, G., Mattioli, E., Pittet, B., Lécuyer, C., Suchéras-Marx, B., Duarte, L.V., Philippe M., Reggiani, M.L., Martineau, F., 2010. Secular environmental precursors to Early Toarcian (Jurassic) extreme climate changes. Earth Planet. Sci. Lett. 290, 448–458.
Suan, G., Mattioli, E., Pittet, B., Mailliot, S., Lécuyer, C., 2008a. Evidence for major environmental perturbation prior to and during the Toarcian (Early Jurassic) oceanic anoxic event from the Lusitanian Basin, Portugal. Paleoceanography 23, PA1202, doi:10.1029/2007PA001459.
Suan, G., Nikitenko, B.L., Rogov, M.A., Baudin, F., Spangenberg, J.E., Knyazev, V.J., Glinskikh, L.A., Goryacheva, A.A., Adatte, T., Riding, J.B., Föllmi, K.B., Pittet, B., Mattioli, E., Lécuyer, C., 2011. Polar record of Early Jurassic massive carbon injection. Earth Planet. Sci. Lett. 312, 102–113.
Suan, G., Pittet, B., Bour, I., Mattioli, E., Duarte, L.V., Mailliot, S., 2008b. Duration of the Early Toarcian carbon isotope excursion deduced from spectral analysis: consequence for its possible causes. Earth Planet. Sci. Lett. 267, 666–679.
Svensen, H., Corfu, F., Polteau, S., Hammer, Ø., Planke, S., 2012. Rapid magma emplacement in the Karoo Large Igneous Province. Earth Planet. Sci. Lett. 325–326, 1–9.
Svensen, H., Planke, S., Chevallier, L., Malthe-Sørenssen, A., Corfu, F., Jamtveit, B., 2007. Hydrothermal venting of greenhouse gases triggering Early Jurassic global warming. Earth Planet. Sci. Lett.256, 554–566.
Them, T.R., Gill, B.C., Caruthers, A.H., Gröcke, D.R., Gerhardt, A.M., Gröcke, D.R., Lyons, T.W., Marroquin, S.M., Nielsen, S.G., Trabucho Alexandre, J.P., Owens, J.D., 2018. Thallium isotopes reveal protracted anoxia during the Toarcian (Early Jurassic) associated with volcanism, carbon burial, and mass ex-tinction. Proc. Natl. Acad. Sci.115, 6596–6601.
Them, T.R., Gill, B.C., Caruthers, A.H., Gröcke, D.R., Tulsky, E.T., Martindale, R.C., Poulton, T.P., Smith, P.L., 2017b. High-resolution carbon isotope records of the Toarcian Oceanic Anoxic Event (Early Jurassic) from North America and implications for the global drivers of the Toarcian carbon cycle. Earth Plan. Sci. Lett 459, 118–126.
Them, T.R., Gill, B.C., Selby, D., Gröcke, D.R., Friedman, R.M., Owens, J.D., 2017a. Evidence for rapid weathering response to climatic warming during the Toarcian Oceanic Anoxic Event. Scientific Reports 7, no. 5003, 10p. doi:10.1038/s41598-017-05307-y.
Thierry, J., Abbate, A.S., Alekseev, O.R. et al., 2000. Middle Toarcian. In: Atlas Peri-Tethys Paleogeographical Maps, Eds.: J. Dercourt, M. Gaetani, B. Vrielynck, E.B. Barrier, B. Biju-Duval, M.-F. Brunet, J.P. Caldet, S. Crasquin and M. Sandules), Vol. I–XX. CCGM/CGMW, Paris, map 8 (40 co-authors).
Thomson, D.J., 1982. Spectrum estimation and harmonic analysis. IEEE Proc. 70, 1055–1096.
Trecalli, A., Spangenberg, J., Adatte, T., Follmi, K.B., Parente, M., 2012. Carbonate platform evidence of ocean acidification at the onset of the early Toarcian oceanic anoxic event. Earth Planet. Sci. Lett. 357-358, 214–225.

Tremolada, F., van de Schootbrugge, B., Erba, E., 2005. Early Jurassic schizosphaerellid crisis in Cantabria, Spain: implications for calcification rates and phytoplankton evolution across the Toarcian oceanic anoxic event. Paleoceanography 20, PA2011.

van de Schootbrugge, B., McArthur, J.M., Bailey, T.R., Rosenthal, Y., Wright, J.D., Miller K.G., 2005. Toarcian oceanic anoxic event: An assessment of global causes using belemnite C isotope records. Paleoceanography 20, PA3008, doi:10.1029/2004PA001102.

Wang, Y., Mosbrugger, V., Zhang, H., 2005. Early to Middle Jurassic vegetation and climatic events in the Qaidam Basin, northwest China. Palaeogeogr. Palaeoclimatol. Palaeoecol. 224, 200–216.

Wilmsen, M., Neuweiler, F., 2008. Biosedimentology of the Early Jurassic post-extinction carbonate depositional system, central High Atlas rift basin, Morocco. Sedimentology 55, 773–807.

Xu, W., Ruhl, M., Jenkyns, H.C., Leng, M.J., Huggett, J.M., Minisini, D., Ullmann, C.V., Riding, J.B., Weijers, J.W.H., Storm, M.S., Percival, L.M.E., Tosca, N.J., Idiz, E.F., Tegelaar, E.W., Hesselbo, S.P., 2018. Evolution of the Toarcian (Early Jurassic) carbon cycle and global climatic controls on local sedimentary processes (Cardigan Bay Basin, UK). Earth and Planetary Science Letters, 484, 396–411.

Zeebe, R.E., Zachos, J.C., Dickens, G.R., 2009. Carbon dioxide forcing alone insufficient to explain Palaeocene-Eocene Thermal Maximum warming. Nature Geoscience 2(8), 576–580, doi:10.1038/ngeo578.

Figure 1: Present and Toarcian location of the Talghemt section. **(A)** Palaeogeographic map of Western Tethys area during the Toarcian (after Thierry et al., 2000, modified by Merino-Tomé et al., 2012) showing the location of the High Atlas (HA) (Morocco), the Lusitanian Basin (LUS) (Portugal), the Paris Basin (PAR) (France) and the United Kingdom (UK). The red-dashed rectangle roughly indicates the expanded view in 'B', but for the present location. **(B)** Simplified structural map of Morocco (after Lachkar et al., 2009, modified by Bodin et al., 2010) showing the location of the Talghemt studied section (indicated by a red star) and Amellago section (Bodin et al., 2010) (indicated by a black star). The Atlas range is colored in brown.

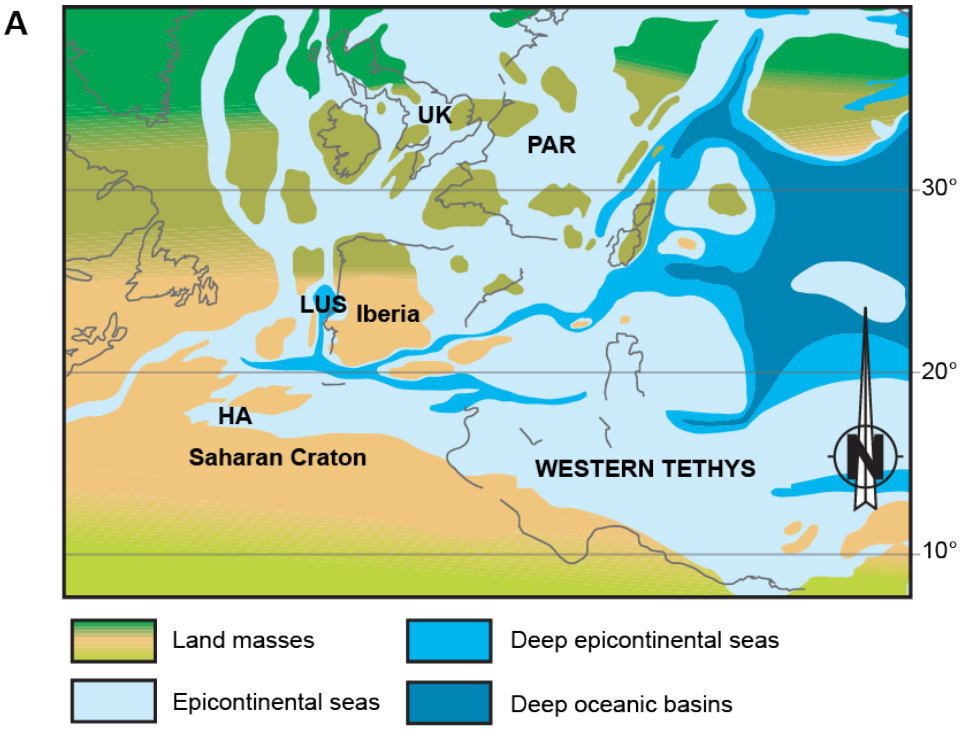

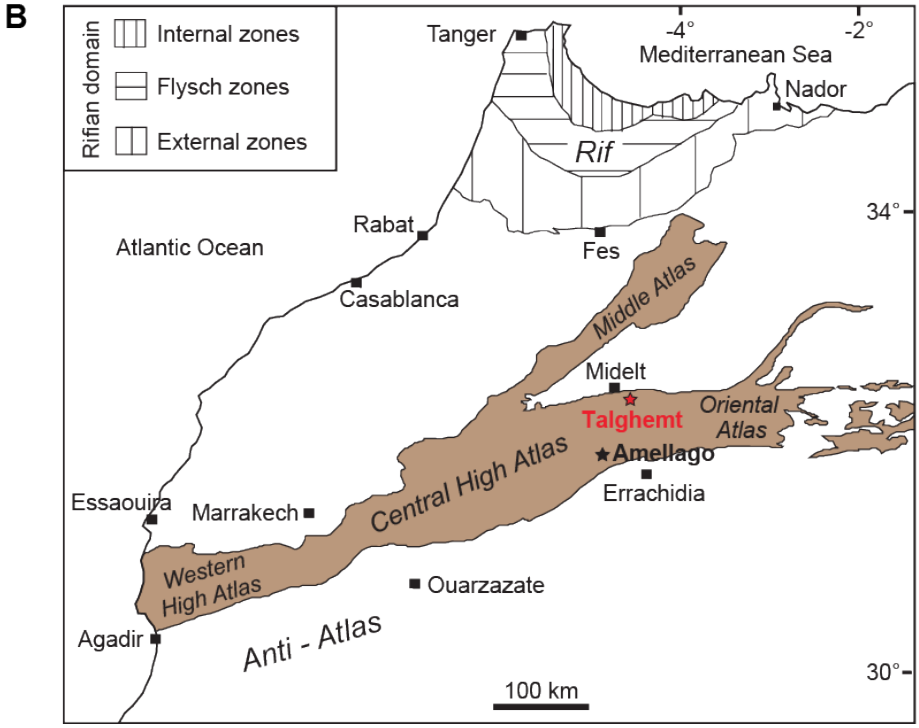

Figure 2: Bio-lithostratigraphy and sedimentological description of the Talghemt section. **(A)** Main Jurassic sedimentary formations in the Talghemt outcropping area (Sadki et al., 1999). **(B)** Bio-lithostratigraphy and sedimentological description of the studied Talghemt section. **(C)** Expanded view of the the Pliensbachian-Toarcian transition along with ammonite distribution (see Plates 1 and 2). The stratigraphic positions of ammonite taxa identified on Plates 1 and 2 are referred to the numbers of beds (Column 'Bed number' in 'C').

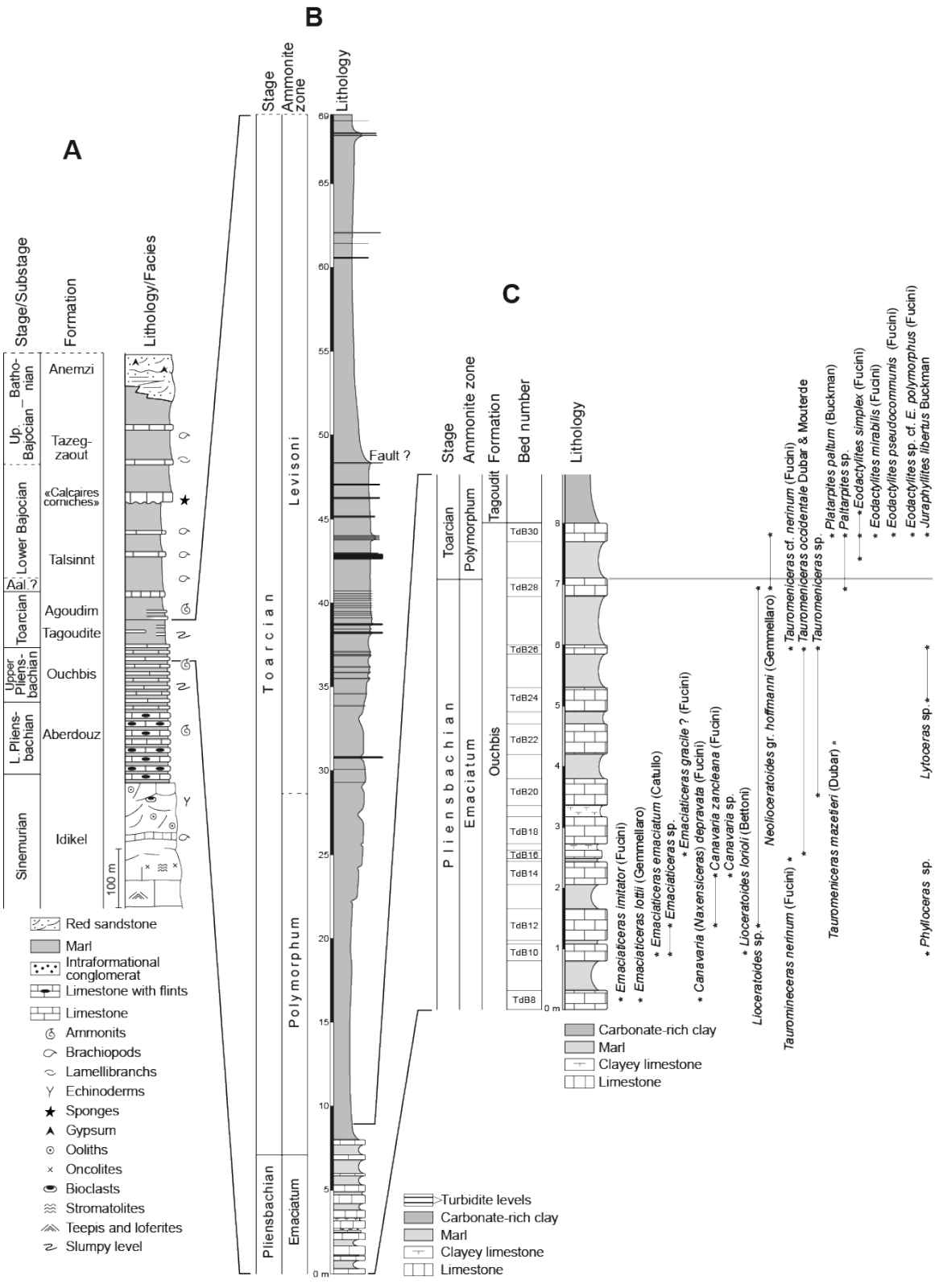

Figure 3: Integrated bio-lithostratigraphy, carbonate content (%$CaCO_3$) and stable carbon isotopes ($d^{13}C$) at Talghemt section (High Atlas, Morocco). The Polymorphum/Levisoni boundary was tentatively placed by Sadki (1996) at around 30 m, according to turbidite occurrence (dashed line with question mark), and replaced here at around 40 m (dashed line) according to $d^{13}C$ correlation with Peniche (see Fig. 8). The Pliensbachian-Toarcian (Pl-To) boundary event, and the Toarcian Oceanic Anoxic Event (T-OAE) along with two possible interpretations are shown. The option of the uppermost boundary of CIE does not correspond to the seemingly $d^{13}C$ outlier (at ~52 m). We have fixed the end of CIE on the basis of the smoothed $d^{13}C$ data, which shows less noise than the raw data (see Fig. 10A). For the lithological description see Fig. 2 and Section 1.2.

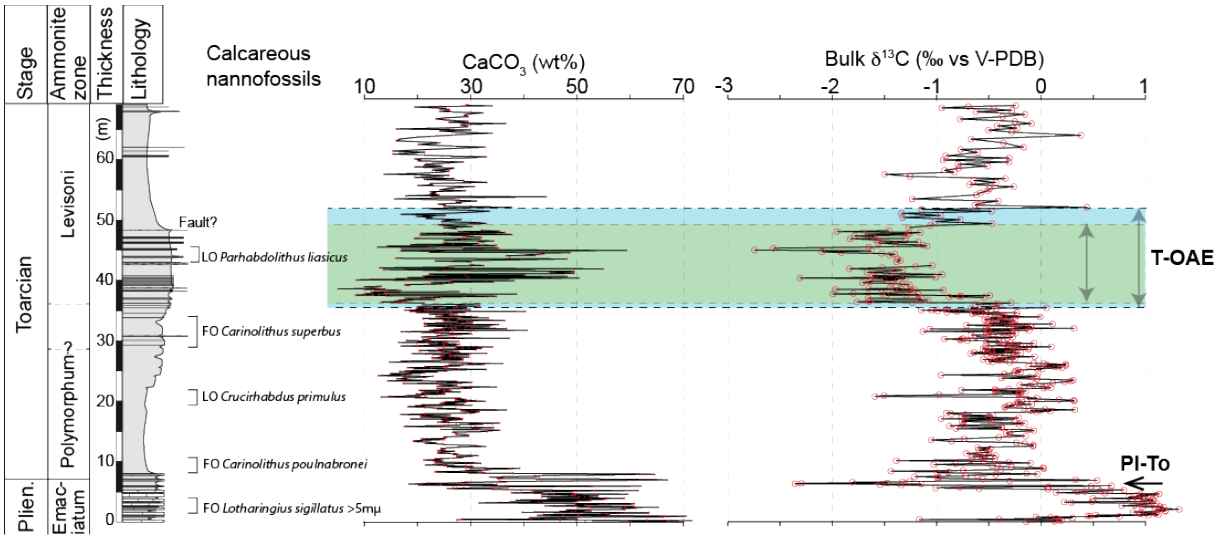

Figure 4: Power spectra of %$CaCO_3$ and $d^{13}C$ Talghemt data in the stratigraphic domain. **(A)** Power spectrum of %$CaCO_3$ data. **(B)** Power spectrum of $d^{13}C$ data. Abbreviations: 'E405' for the 405 kyr eccentricity, 'e100' for the short eccentricity, 'Obl.' for the obliquity and 'Prec.' for the precession.

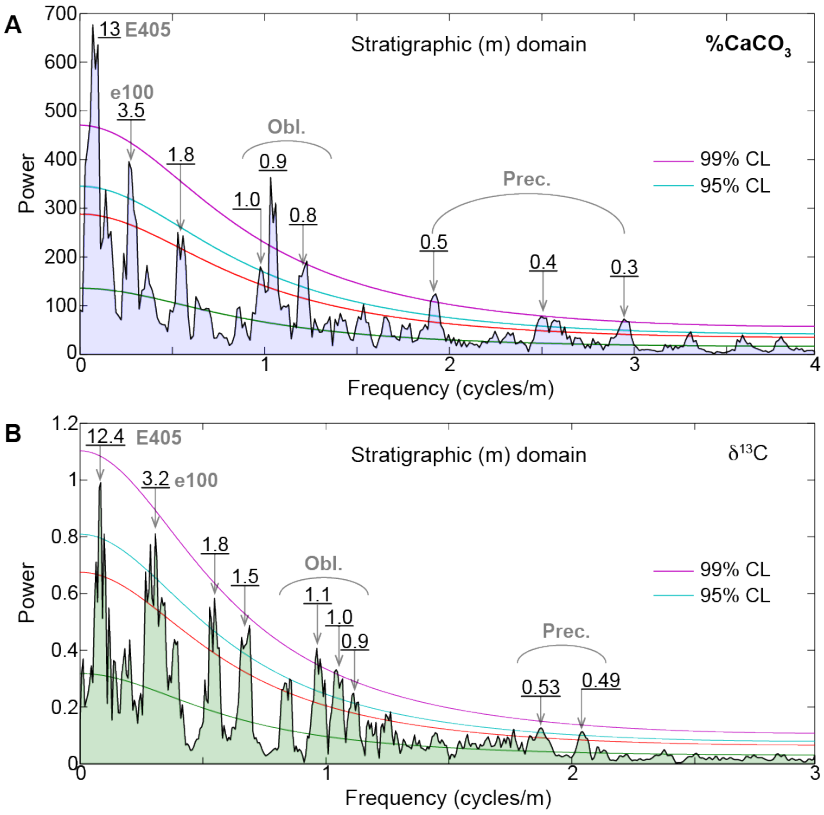

Figure 5: Power spectra of %$CaCO_3$ and d^{13}C Talghemt data in the time domain (405 and 110 kyr eccentricity tunings). **(A)** Power spectra of the tuned %$CaCO_3$ data. **(B)** Power spectra of the tuned d^{13}C data. Abbreviations: 'E405' for the 405 kyr eccentricity, 'e100' for the short eccentricity, 'Obl.' for the obliquity and 'Prec.' for the precession.

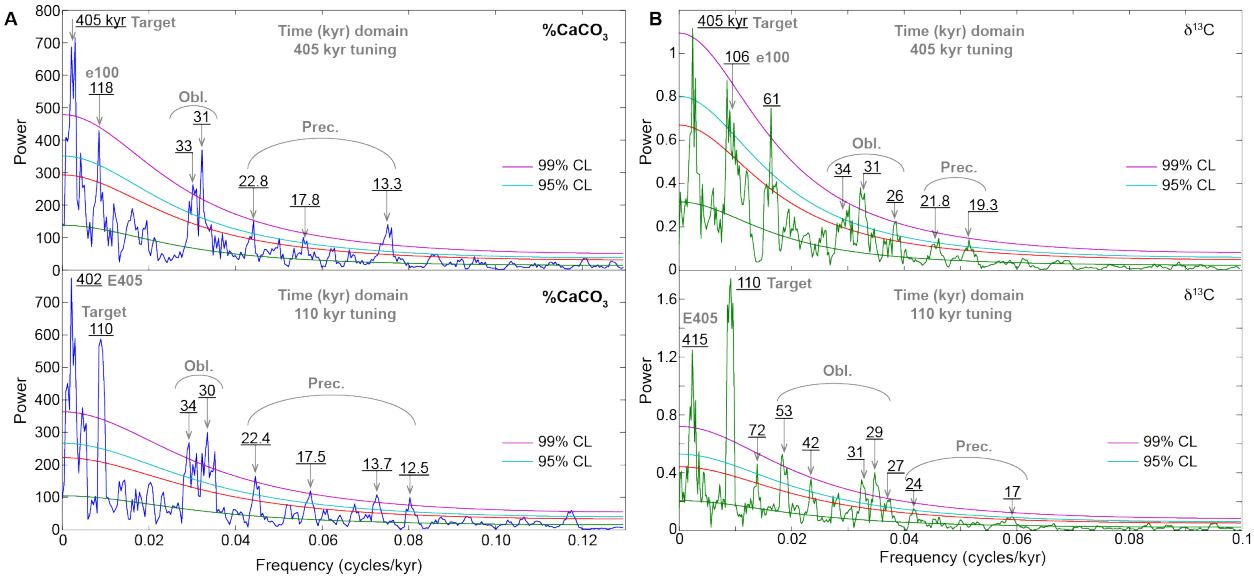

Figure 6: Spectra of obliquity tunings performed at different values of O1 period in order to seek for the best calibrated g2-g5 related eccentricity term at 405 kyr (Laskar et al., 2004). Each obliquity tuned time series was 1x zero-padded before spectral analysis. Note the optimal O1 obliquity tuning is at around ~30 kyr, which provides a period of 405 kyr for g2-g5 and a mean short eccentricity of 112 kyr. Abbreviations: 'E405' for the 405 kyr (g2-g5) stable eccentricity, 'e100' for the short eccentricity, 'O1' for the main obliquity period.

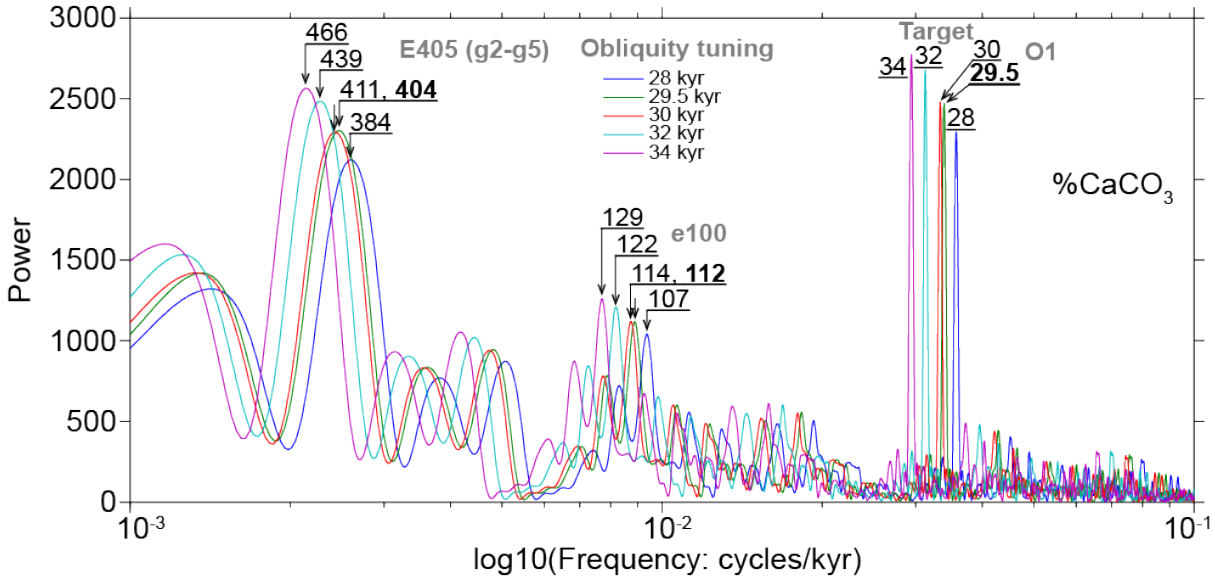

Figure 7: Bandpass filtering of the detected astronomical cycles in the 405 kyr tuned %$CaCO_3$ and $d^{13}C$ data of Talghemt section, along with the Pliensbachian-Toarcian (Pl-To) boundary event and the Toarcian Oceanic Anoxic Event (T-OAE). $d^{13}C$ time series is anchored to %$CaCO_3$ timescale. The total duration of the studied interval is ~2250 kyr. Two possible interpretations of the T-OAE CIE provide durations of ~400 and ~500 kyr. Note that there is no coherent phase relationship at the 405 kyr band between %$CaCO_3$ and $d^{13}C$, possibly because of the effect of events on long-term $d^{13}C$ cycling. However, an exceptional phase relationship could be seen at the obliquity and short eccentricy bands: the two %$CaCO_3$ and $d^{13}C$ proxies are in phase outside the T-OAE, but out of phase within the T-OAE (Section 3.2).

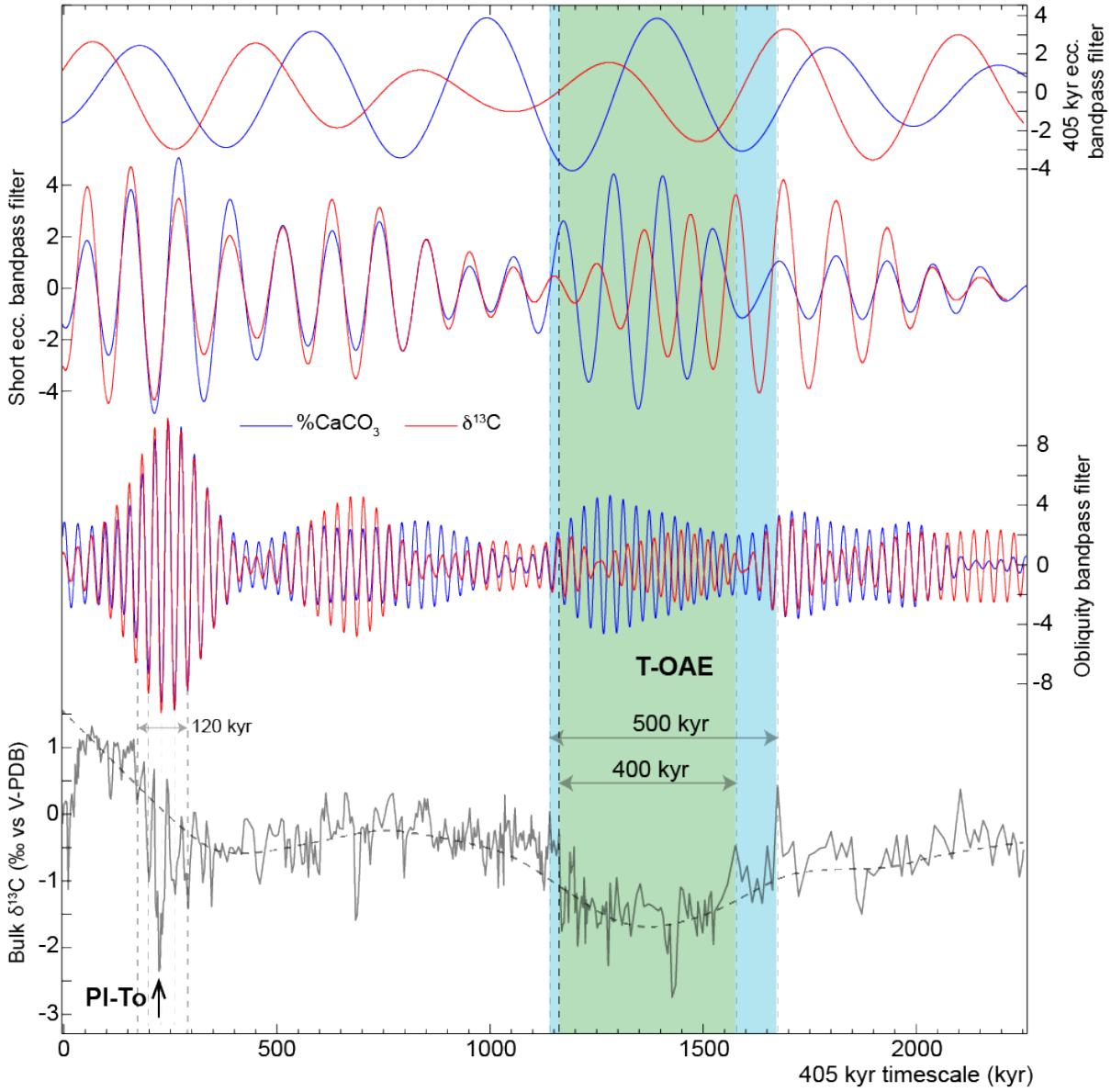

Figure 8: Stable carbon isotopes ($d^{13}C$) and sedimentological correlation between Talghemt and Peniche sections **(A)** and $d^{13}C$ correlation between Talghemt, Peniche, Sancerre and Yorkshire **(B)**. Note that the two sections Talghemt and Peniche in 'A' are reset to the same stratigraphic scale. Talghemt data are from the present study. Peniche bulk carbonate $d^{13}C$ data are from Hesselbo et al. (2007). Sancerre bulk carbonate $d^{13}C$ data are from Hermoso et al. (2009, 2012, 2013). Yorkshire organic carbon $d^{13}C$ data are from Kemp et al. (2005) and Cohen et al. (2004).

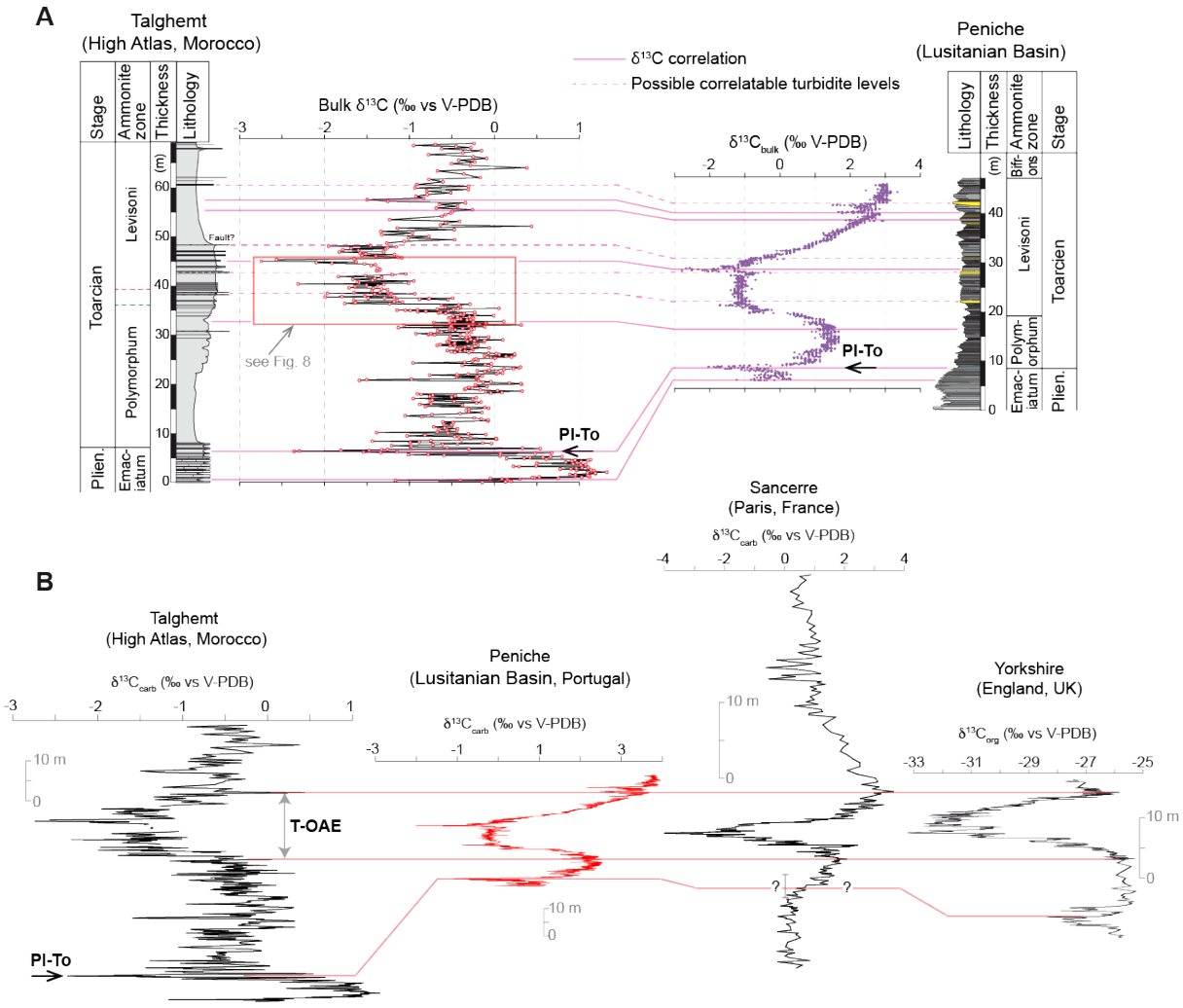

Figure 9: Spectral analysis of Peniche $d^{13}C$ data per intervals. Erosional discontinuities are according to Pittet et al. (2014). Precession bandpass filters are in green, and obliquity bandpass filters are in red. Note that the period ratio of the two strongest peaks within the three analyzed intervals is nearly 1/2 (precession over obliquity periods), which may correspond to the ratio of precession over the obliquity (see also figure 6 of Boulila and Hinnov, 2017). Obliquity cycles are numbered from 1 to 25. Note that the CIE of T-OAE includes 15 to 17 obliquity cycles. At Talghemt, the equivalent interval includes 16 to 17 obliquity cycles (see Fig. 7 and Section 3.2). Peniche bulk carbonate $d^{13}C$ data are from Hesselbo et al. (2007). The ~1.4 m related obliquity peak in $\%CaCO_3$ data (Kemp et al., 2011; Boulila and Hinnov, 2017) is the average of the three peaks 1.2 m, 1.2 m and 1.7 m in the three intervals I1, I2 and I3 respectively.

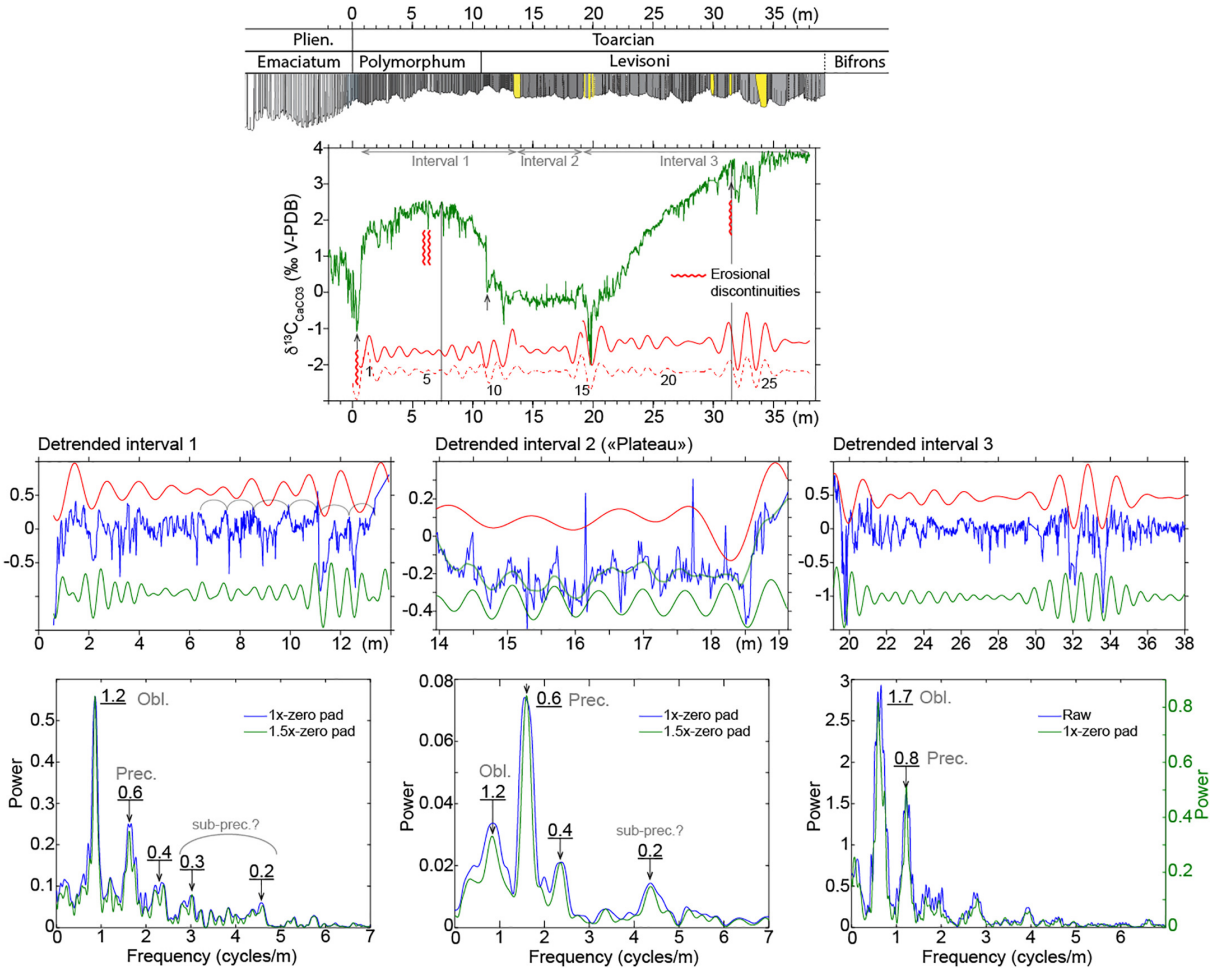

Figure 10: (A) High-resolution $d^{13}C$ correlation between Talghemt (Morocco) and Peniche (Portugal) sections. The Talghemt $d^{13}C$ data are 5-point smoothed (moving average) to highlight the end of CIE. The decreasing part of CIE (T-OAE) is dominated by the obliquity, while its increasing part is dominated by the short eccentricity. **(B)** High-resolution $d^{13}C$ correlation at the dreceasing part of CIE (T-OAE) between Talghemt, Peniche, Sancerre (Paris) and Yorkshire (England). Numbers 1 through 7 are short-term oscillations in $d^{13}C$, which have been ascribed to high-frequency obliquity cycles (Boulila et al., 2014; Boulila and Hinnov, 2017, and the present study from Talghemt section). The '*Plateau*' hypothesis at Talghemt is unlikely because there is a mismatch in the obliquity cycles between Peniche and Talghemt. The onset of CIE is placed with uncertainty within one obliquity $d^{13}C$ related cycle. For 'asymmetric' cycles see Boulila and Hinnov (2017). The sources of the used data are referred in Figure 8 caption.

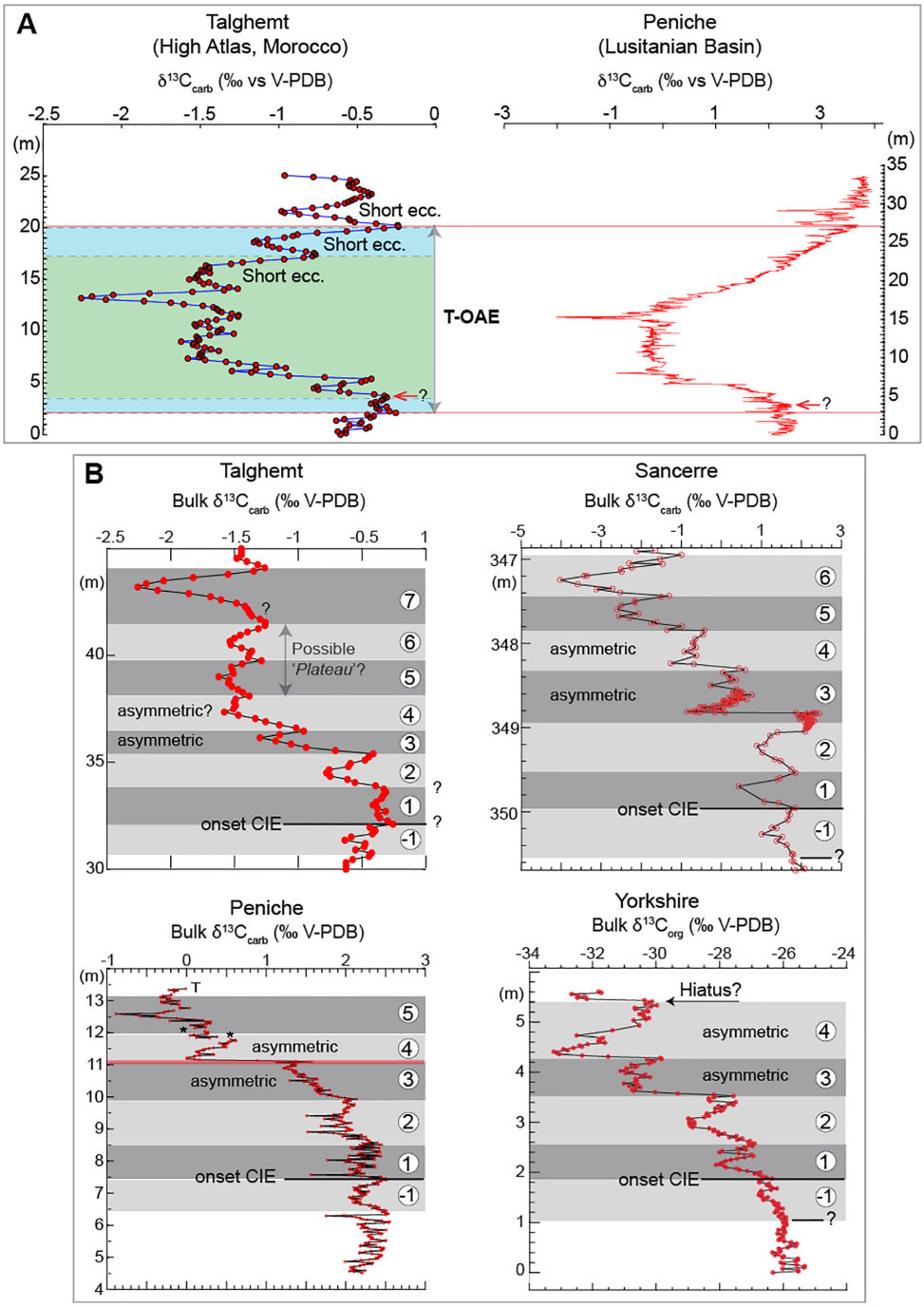
A
Talghemt
(High Atlas, Morocco)
δ13Ccarb (‰ vs V-PDB)
-2.5 -2 -1.5 -1 -0.5 0
(m)
25 20 15 10 5 0
Short ecc.
Short ecc.
Short ecc.
T-OAE
?
Peniche
(Lusitanian Basin)
δ13Ccarb (‰ vs V-PDB)
-3 -1 1 3
(m)
35 30 25 20 15 10 5 0
?
B
Talghemt
Bulk δ13Ccarb (‰ V-PDB)
-2.5 -2 -1.5 -1 -0.5 1
(m)
40 35 30
?
Possible
'Plateau'?
asymmetric?
asymmetric
onset CIE
7 6 5 4 3 2 1 -1
Sancerre
Bulk δ13Ccarb (‰ V-PDB)
-5 -3 -1 1 3
347
(m)
348 349 350
asymmetric
asymmetric
onset CIE
6 5 4 3 2 1 -1
?
Peniche
Bulk δ13Ccarb (‰ V-PDB)
-1 0 1 2 3
(m)
13 12 11 10 9 8 7 6 5 4
T
asymmetric
asymmetric
onset CIE
5 4 3 2 1 -1
Yorkshire
Bulk δ13Corg (‰ V-PDB)
-34 -32 -30 -28 -26 -24
(m)
5 4 3 2 1 0
Hiatus?
asymmetric
asymmetric
onset CIE
4 3 2 1 -1
?

Supplementary Figures and Plates

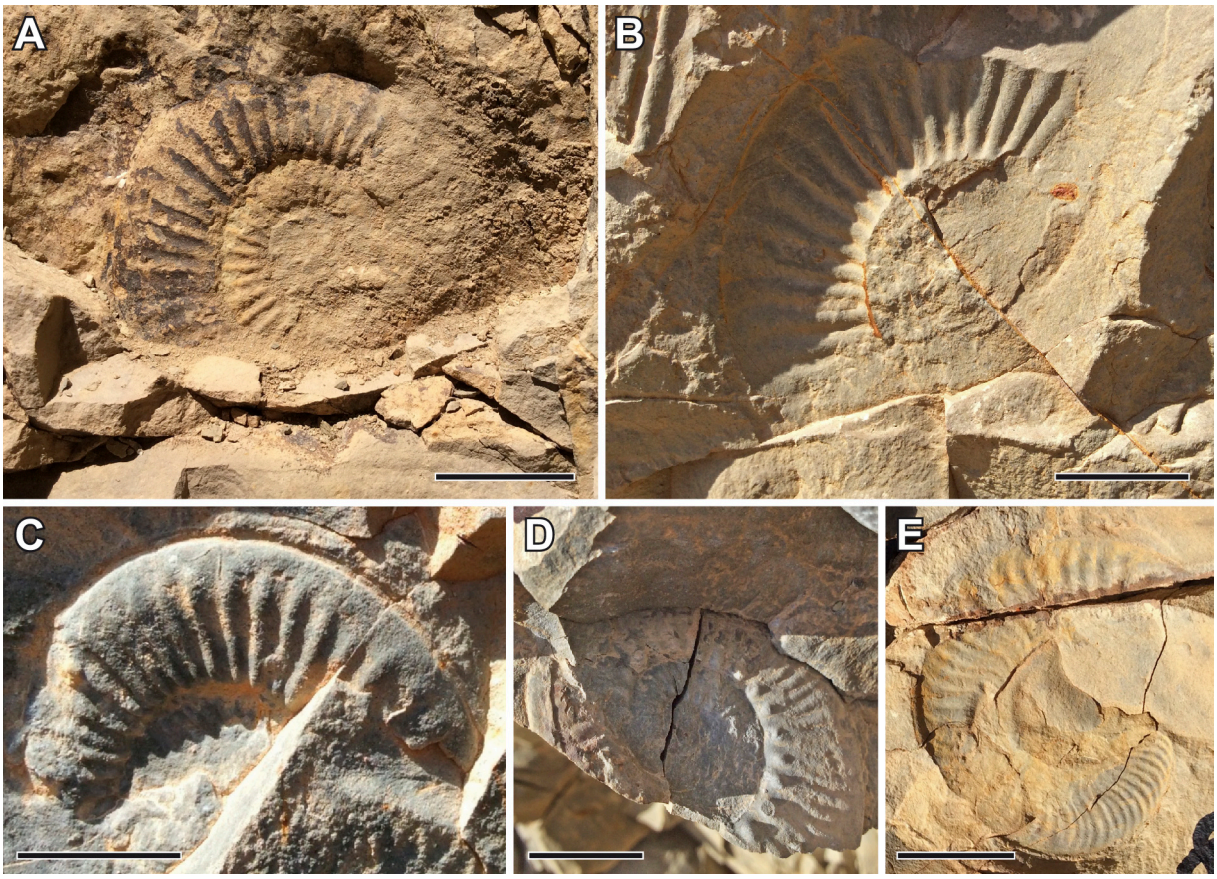

Plate 1: Upper Pliensbachian ammonites from Talghemt section. Scale bar = 1 cm. All beds (TdB, see Fig. 2) where ammonites were found are indicated below. **(A)** *Emaciaticeras lottii* (GEMMELLARO) – Bed TdB8. **(B)** *Emaciaticeras* cf. *imitator* (FUCINI) – Bed TdB8. **(C)** *Canavaria zancleana* (FUCINI) – TdB12. **(D)** *Tauromeniceras mazetieri* (DUBAR) - TdB22. **(E)** *Neolioceratoides* aff. *hoffmanni* (GEMMELLARO) – TdB28.

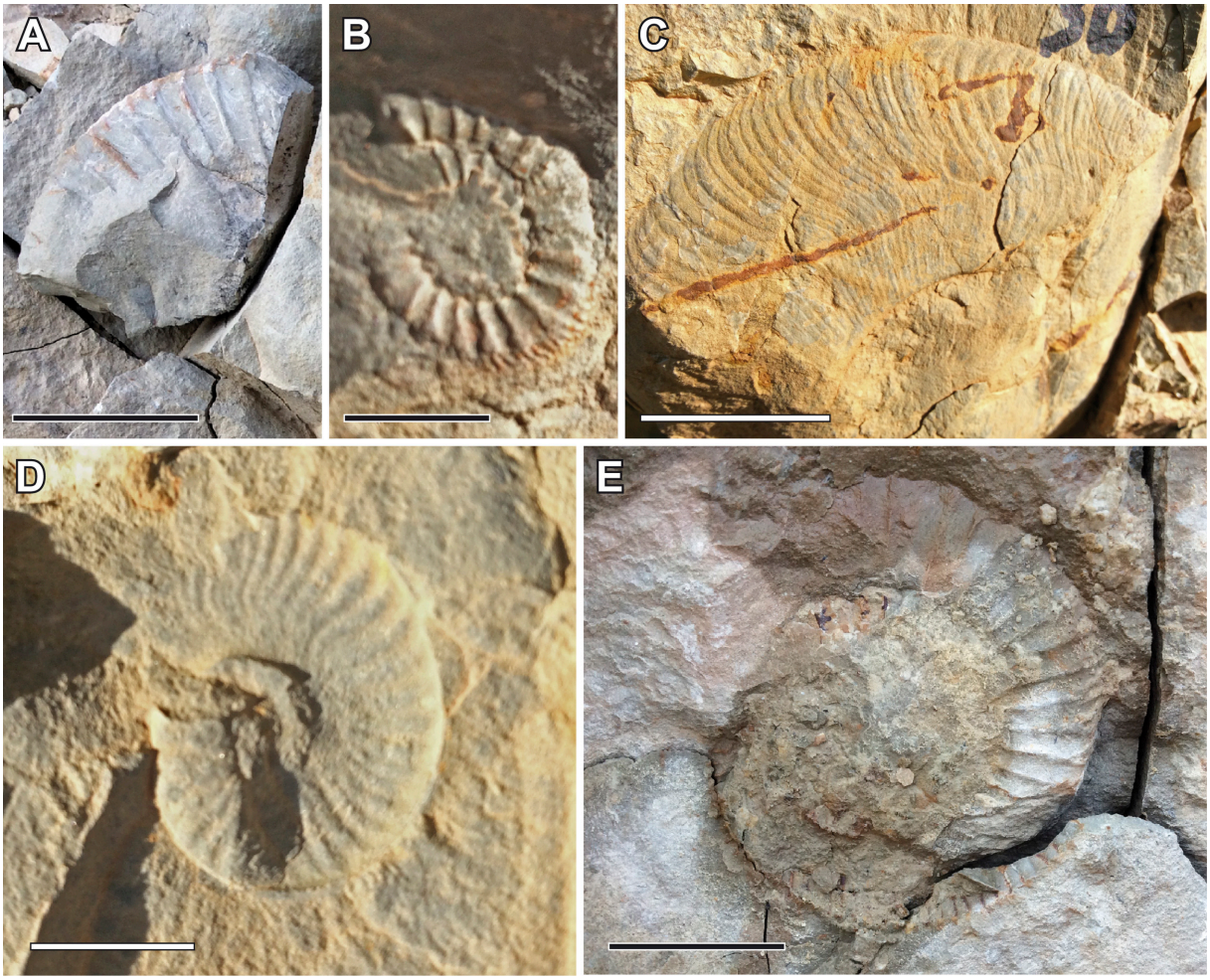

Plate 2: Lower Toarcian ammonites from Talghemt section. Scale bar = 1 cm. All beds (TdB, see Fig. 2) where ammonites were found are indicated below. **(A)** *Eodactylites* sp. - TdB29. **(B)** *Eodactylites simplex* (FUCINI) - TdB30. **(C)** *Paltarpites* sp - TdB30. **(D)** *Neolioceratoides* gr. *hoffmanni* (GEMMELLARO) - TdB30. **(E)** *Eodactylites simplex* (FUCINI) - TdB31.

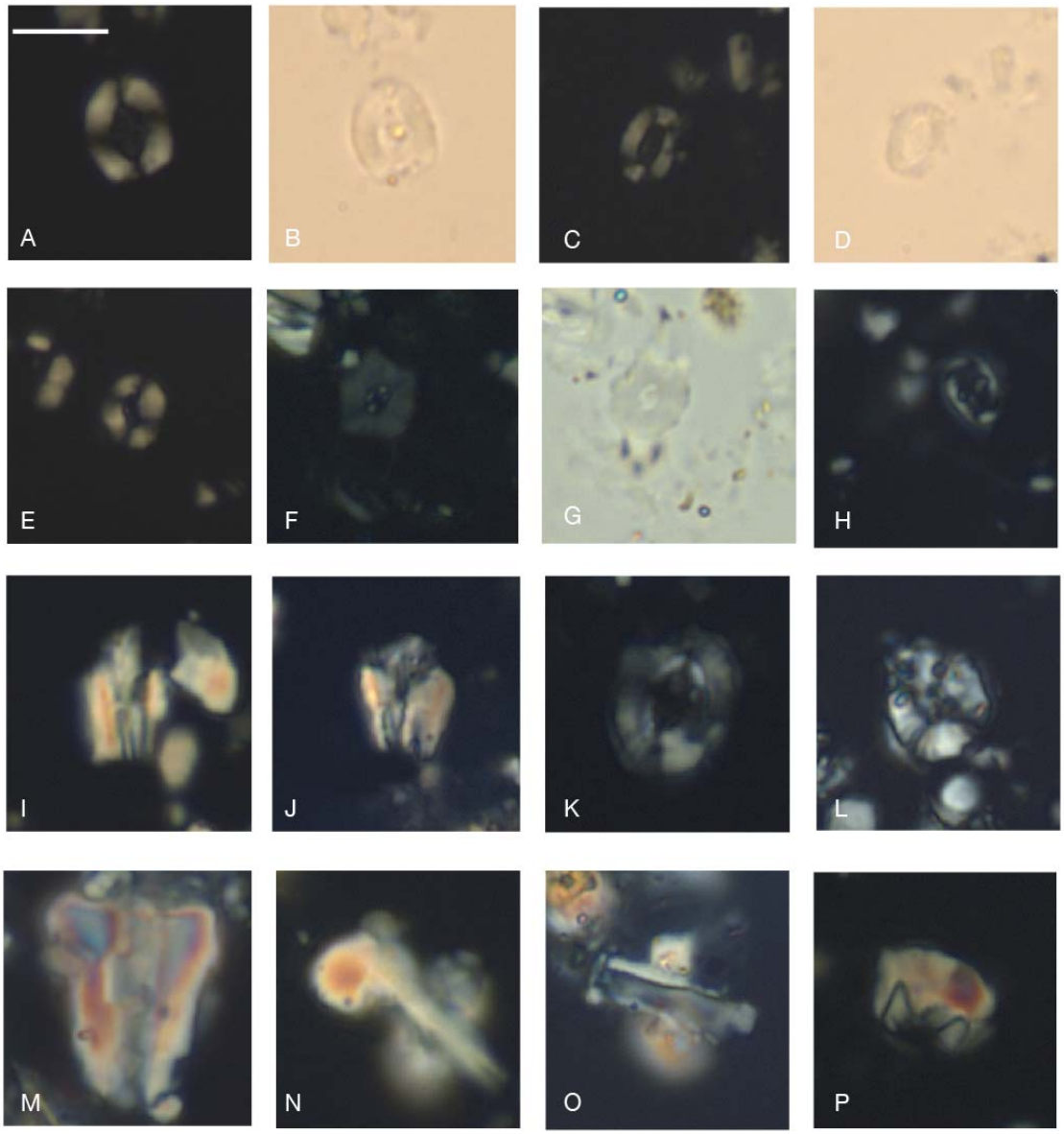

Plate 3: Micrographs of calcareous nannofossil species from Talghemt section. Scale bar = 5 µm. All stratigraphic levels of the corresponding samples are indicated in meter (m) between brackets. A: *Lotharingius sigillatus*, crossed nicols (0.4 m). B: Same specimen as A, natural light. C: *Lotharingius barozii*, crossed nicols (4.8 m). D: Same specimen as C, natural light. E: *Lotharingius hauffii, sample* (22 m). F: *Similiscutum cruciulus*, crossed nicols (57.9 m). G: Same specimen as F, natural light. H: *Crucirhabdus primulus*, crossed nicols (4.8 m). I-J: *Calcivascularis jansae*, crossed nicols (3.2 m). K: *Biscutum grande*, crossed nicols (21 m). L: *Biscutum finchii*, crossed nicols (0.4 m). M: *Calyculus noelae*, crossed nicols (4 m). N: *Carinolithus superbus*, crossed nicols (30.2 m). O: *Carinolithus poulnabronei*, crossed nicols (38.9 m). P: *Mitrolithus lenticularis*, crossed nicols (21.7 m).

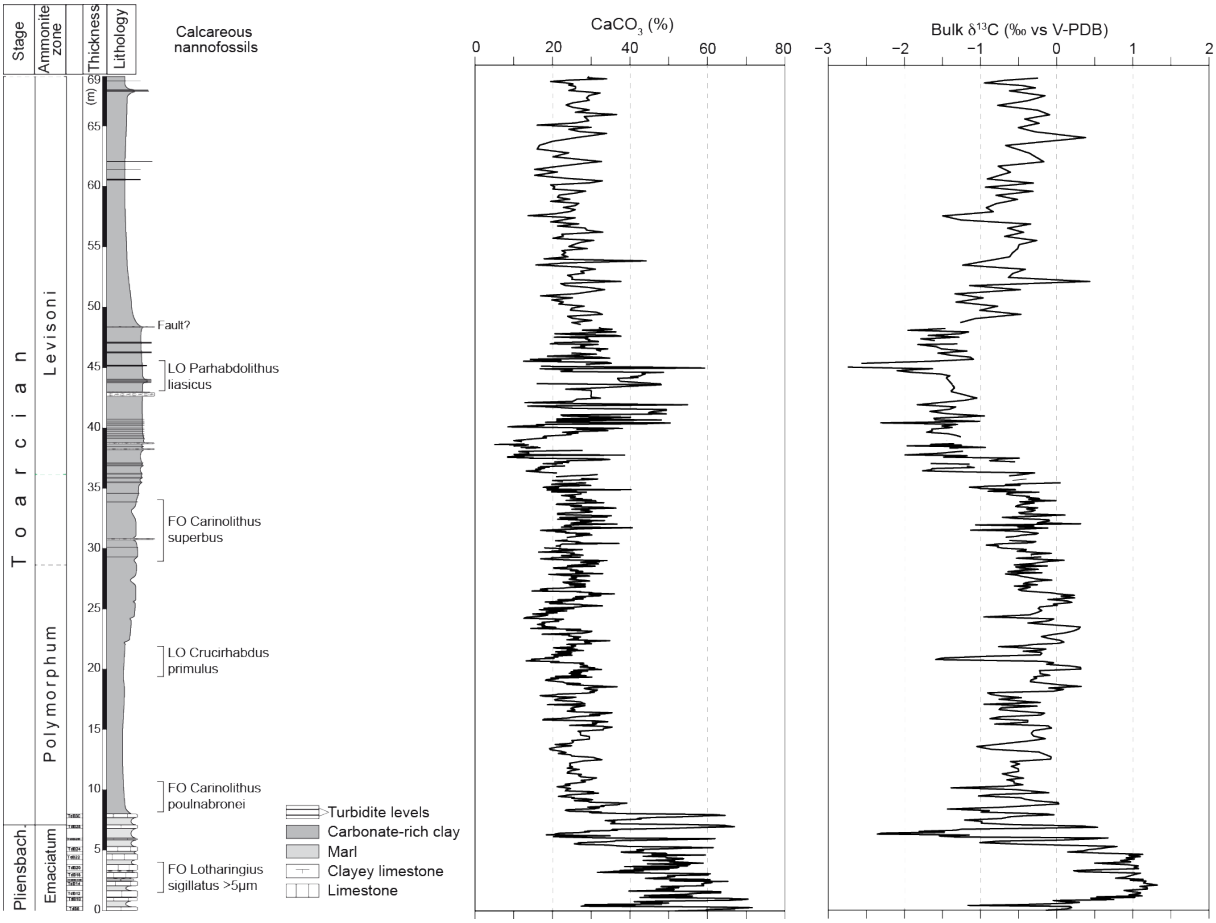

Figure S1: Bio-lithostratigraphic and geochemical data of Talghemt section.

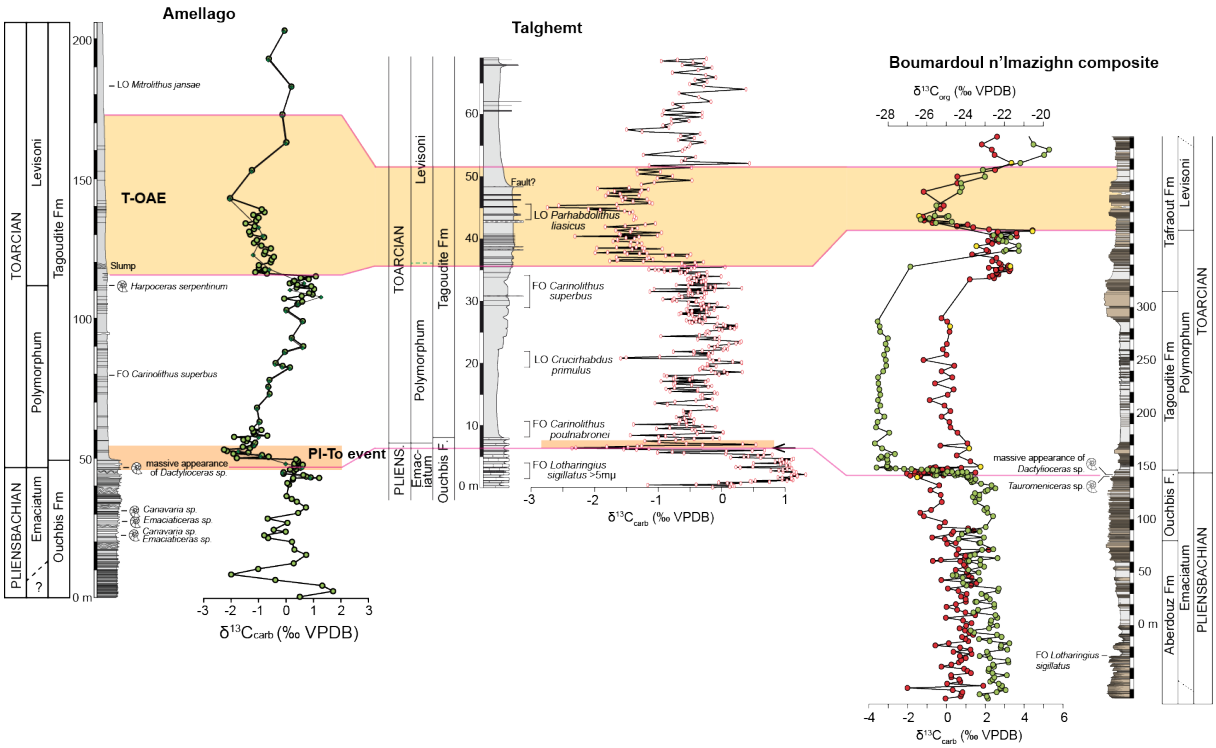

Figure S2: Correlation of the Pliensbachian-Toarcian (Pl-To) transition event and the T-OAE between Talghemt (present study), Amellago and Boumardoul n'Imazighn sections (Bodin et al., 2016).